UC Berkeley
UC Berkeley Previously Published Works

Title

Responses of Marginal and Intrinsic Water-Use Efficiency to Changing Aridity Using FLUXNET Observations

Permalink

https://escholarship.org/uc/item/54m1b3t8

Journal

Journal of Geophysical Research Biogeosciences, 129(6)

ISSN

2169-8953

Authors

Yi, Koong

Novick, Kimberly A

Zhang, Quan

et al.

Publication Date

2024-06-01

DOI

10.1029/2023jg007875

Copyright Information

Peer reviewed

Responses of marginal and intrinsic water-use efficiency to changing aridity using FLUXNET observations

Koong Yi[1], Kimberly A. Novick[2], Quan Zhang[3], Lixin Wang[4], Taehee Hwang[5], Xi Yang[6], Kanishka Mallick[7,8], Martin Béland[7,9], Gabriel B. Senay[10], Dennis Baldocchi[7]

[1]Earth and Environmental Sciences Area, Lawrence Berkeley National Laboratory, CA, U.S.A.

[2]O'Neill School of Public and Environmental Affairs, Indiana University Bloomington, Bloomington, IN, U.S.A.

[3]State Key Laboratory of Water Resources and Hydropower Engineering Science, Wuhan University, Wuhan, China.

[4]Department of Earth Sciences, Indiana University-Purdue University Indianapolis (IUPUI), Indianapolis, IN, U.S.A.

[5]Department of Geography, Indiana University Bloomington, Bloomington, IN, U.S.A.

[6]Department of Environmental Sciences, University of Virginia, Charlottesville, VA, U.S.A.

[7]Department of Environmental Science, Policy, and Management, University of California, Berkeley, CA, U.S.A.

[8]Department of Environment Research and Innovation, Luxembourg Institute of Science and Technology, Belvaux, Luxembourg

[9]Department of Geomatics Sciences, Laval University, Quebec City, Quebec, Canada

[10]U.S. Geological Survey Earth Resources Observation and Science Center, North Central Climate Adaptation Science Center, Fort Collins, CO, U.S.A.

24   Corresponding Author:

25   Koong Yi

26   Email: koongyi@gmail.com

27   Phone: +1-812-650-2930

28

29   **Abstract**

30   According to classic stomatal optimization theory, plant stomata are regulated to

31   maximize carbon assimilation for a given water loss. A key component of stomatal optimization

32   models is marginal water-use efficiency (mWUE), the ratio of the change of transpiration to the

33   change in carbon assimilation. Although the mWUE is often assumed to be constant, variability

34   of mWUE under changing hydrologic conditions has been reported. However, there has yet to be

35   a consensus on the patterns of mWUE variabilities and their relations with atmospheric aridity.

36   We investigate the dynamics of mWUE in response to vapor pressure deficit (VPD) and aridity

37   index using carbon and water fluxes from 115 eddy covariance towers available from the global

38   database FLUXNET. We demonstrate a non-linear mWUE-VPD relationship at a sub-daily scale

39   in general; mWUE varies substantially at both low and high VPD levels. However, mWUE

40   remains relatively constant within the mid-range of VPD. Despite the highly non-linear

41   relationship between mWUE and VPD, the relationship can be informed by the strong linear

42   relationship between ecosystem-level inherent water-use efficiency (IWUE) and mWUE using

43   the slope, m^*. We further identify site-specific m^* and its variability with changing site-level

44   aridity across six vegetation types. We suggest accurately representing the relationship between

45   IWUE and VPD using Michaelis-Menten or quadratic functions to ensure precise estimation of

46   mWUE variability for individual sites.

Plain Language Summary

Plants use diverse strategies for water utilization during growth. Marginal water-use efficiency (mWUE) quantifies how effectively plants gain carbon relative to the water they lose through their leaves. A scientific debate exists regarding how mWUE responds to dry conditions. To investigate this, we analyze data from various vegetation types worldwide, observing changes in mWUE under dry conditions. Contrary to common assumptions, mWUE is not a constant; it varies substantially based on moisture levels. Additionally, we show that a simpler measure called inherent water-use efficiency (IWUE) can help explain this complicated relationship, which is useful for predicting plant growth under different moisture conditions.

Keywords

Climate change, drought, eddy covariance, stomatal optimization theory, vapor pressure deficit, water-use efficiency

Running title

Response of mWUE and IWUE to changing aridity

1. Introduction

Terrestrial plants mitigate global warming by sequestering atmospheric carbon dioxide (CO_2) through photosynthesis (Beer et al., 2010). However, photosynthesis is inherently linked with plant water loss via transpiration, as CO_2 and water vapor share the same stomatal pathway. Plants risk hydraulic damage during droughts if they maintain high stomatal conductance as soil water availability decreases and atmospheric demand increases, resulting in low leaf water potential and xylem cavitation. Therefore, plants must balance stomatal function to optimize carbon uptake while minimizing transpirational water loss and hydraulic stress (Cowan & Farquhar, 1977; Katul et al., 2010; Sperry et al., 2017; Wang et al., 2020). To predict plant ecophysiological responses to projected changes in atmospheric CO_2 concentration, elevated atmospheric water demand, and more severe and frequent drought events, we need a mechanistic understanding of how different ecosystems regulate the trade-off between photosynthetic carbon assimilation and transpirational water loss.

Although carbon uptake is usually represented through mechanistic models of photosynthesis (e.g., the Michaelis-Menten equation (Marshall & Biscoe, 1980; Michaelis & Menten, 1913; Thornley, 1976); the Farquhar model (Von Caemmerer, 2000; Farquhar et al., 1980a)), water use (i.e., transpiration) is often described based on empirical relationships that prescribe how stomatal conductance responds to environmental drivers and carbon uptakes. For example, the Ball-Berry model (Ball et al., 1987) is one of the most widely used empirical stomatal conductance models (Anderegg et al., 2017; Buckley, 2017; Katul et al., 2010), and has been readily incorporated into many climate models (Bonan et al., 2014). It takes the form:

$$g_s = g_0 + g_1 \frac{A}{c_a} \text{RH} \qquad (1)$$

where g_s is stomatal conductance (mol m^{-2} s^{-1}), A is carbon assimilation rate (μmol m^{-2} s^{-1}), c_a is atmospheric CO_2 concentration (ppm), RH is relative humidity at the leaf surface, and g_0 and g_1 are empirically fitted parameters. To simulate the non-linear variation in g_s with changing humidity, Leuning (1995) modified the Ball-Berry model by replacing relative humidity with a vapor pressure deficit (VPD) response function as follows:

$$g_s = g_0 + g_1 \cdot \frac{A}{(c_a - \Gamma^*)\left(1 + \frac{\text{VPD}}{\text{VPD}_0}\right)} \qquad (2)$$

where Γ^* is CO_2 compensation point for photosynthesis (ppm) and VPD_0 is the empirically determined coefficient, representing the slope of the relationship between g_s and VPD. These empirical models are relatively simple, easy to use, and work well for well-watered conditions (Bonan et al., 2014). However, they have an incomplete grounding in physiological theory, leading to uncertainty when they are extrapolated to predict plant function under unprecedented climate conditions (Franks et al., 2018; Knauer et al., 2015, 2018; Medlyn et al., 2012; Sabot et al., 2022).

An alternative way to enable the theoretical interpretation of leaf-level stomatal conductance models is to adopt the principle of stomatal optimization theory (Anderegg et al., 2018; Bonan et al., 2014; Katul et al., 2009; Katul et al., 2010; Medlyn et al., 2012; Novick et al., 2016b; Sperry et al., 2017; Wolf et al., 2016). Stomatal optimization theory was originally based on a hypothesis that stomata are regulated to maximize carbon assimilation (A) for a given water loss (transpiration, E). A key parameter in this class of models is the so-called "marginal water-use efficiency (mWUE)," here defined as the ratio of a change in E to a change in A ($\partial E / \partial A$) following Cowan and Farquhar (1977), although it is sometimes defined as the inverse form ($\partial A / \partial E$) (Katul et al., 2010; Manzoni et al., 2011). The optimality models often maintain the mWUE constant over arbitrary time steps (e.g., daily), assuming abundant water at the canopy

5

109   (Buckley, 2017; Cowan & Farquhar, 1977; Makela et al., 1996). However, this may not hold true

110   at sub-daily timescales, where high atmospheric demand (i.e., VPD) during midday can decrease

111   water potential at the canopy level even when soil moisture is abundant (Anderegg et al., 2017;

112   Grossiord et al., 2020).

113   Understanding how mWUE changes under hydrologic stress is necessary for the

114   optimization models in a prognostic sense, yet no consensus on the magnitude or even direction

115   of these changes exists. For instance, Manzoni et al. (2011) and Zhou et al. (2013, 2014)

116   performed meta-analyses of leaf gas exchange measurements from previous studies that spanned

117   wide ranges of species and moisture conditions. A major difference in their approaches was the

118   proxy for plant water status; Manzoni et al. (2011) used mid-day leaf water potential, whereas

119   Zhou et al. (2013, 2014) used pre-dawn leaf water potential as a proxy for soil moisture

120   availability. Similarly, Lin et al. (2015) compiled a global database of leaf gas exchange

121   measurements spanning diverse plant functional types and estimated a slope parameter (g_1)

122   (Medlyn et al., 2012), which is analogous to the slope parameter from empirical models (Eqs. 1

123   & 2) and proportional to $\sqrt{\partial E / \partial A}$ (Medlyn et al., 2012). They further evaluated the relationship

124   between g_1 and a moisture index, defined as the ratio of mean annual precipitation to the

125   equilibrium evapotranspiration. Mäkelä et al. (1996) and Lu et al. (2016) took a theoretical

126   approach to examine short- and long-term optimal stomatal behavior, respectively, in response to

127   the soil moisture availability assuming that plants are adapted to the stochastic rainfall patterns of

128   their environments. More recently, alternative stomatal optimization perspectives have been

129   proposed, which presume stomata function to maximize carbon uptake while minimizing water

130   costs, including those linked to hydraulic damage during droughts (Anderegg et al., 2018; Sperry

131   et al., 2017; Wolf et al., 2016). Although promising, in contrast to the Medlyn et al. (2012)

132 model, these newer formulations have yet to be integrated into land surface model schemes (but

133 refer to Kennedy et al., 2019, for a study implementing plant hydraulics in the Community Land

134 Model). Although theoretical expectation and many studies indicate decreasing mWUE as water

135 stress drives reductions to g_s, there is some evidence of increasing mWUE under water stress

136 (Farquhar et al., 1980b; Grieu et al., 1988; Zhou et al., 2013), although reasons for this needed to

137 be clarified.

138　　It is also important to note that canopy water status and water potential are not

139 determined solely by the availability of water supply but by the balance between water supply

140 and demand, with VPD as a major force exerted on the canopy by the atmosphere (Manzoni et

141 al., 2011, 2013; Novick et al., 2019). Thus, it is reasonable to expect that mWUE needs to be

142 adjusted with changing atmospheric water demand unless other factors limit the plant response

143 (e.g., compromised hydraulic conductivity under water stress, limited soil moisture availability

144 to plants) (Brodribb et al., 2005; Medlyn et al., 2012). Different plants or ecosystems may adjust

145 differently, resulting in divergent responses of mWUE to changing VPD. Understanding the

146 relationship between mWUE and VPD is important given that VPD is expected to keep

147 increasing in the future, which will exert further water stress on plants (Ficklin & Novick, 2017;

148 Grossiord et al., 2020; Novick et al., 2016a; Zhang et al., 2019). Furthermore, while soil

149 moisture is a stochastic variable due to its dependency on intermittent rainfall, VPD is smoother

150 in time and easier to monitor through various meteorological or gas exchange measurement

151 techniques. Although VPD and soil moisture limit plants' carbon uptake and water use

152 independently (Yi et al., 2019), VPD can be used as a proxy of water stress at a sub-daily scale

153 where VPD plays a primary role in regulating stomatal regulation unless severe soil moisture

154 deficiency, as indicated by the models with sub-daily timesteps (e.g., Ball-Berry model and its

155 variations), and in turn influencing the balance between carbon uptake and water loss (i.e., water-

156 use efficiency) at a sub-daily scale (Baldocchi et al., 2022; Grossiord et al., 2020; Novick et al.,

157 2016a). Therefore, examining the association between mWUE and VPD would add insight into

158 the predictability of soil moisture alone.

159   The objectives of this study are (1) to investigate the variation of mWUE at an hourly

160 timescale in response to changing VPD and (2) to explore approaches for estimating mWUE

161 explicitly from the modeled relationship between intrinsic water-use efficiency (iWUE, carbon

162 assimilation per unit stomatal conductance, representing water-use efficiency at leaf level) and

163 VPD. The Ball-Berry model (Eq. 1) reveals that the parameter g_1, which is proportional to

164 $\sqrt{\partial E / \partial A}$ (Medlyn et al., 2012), is related to A/g_s (= iWUE at leaf level). The iWUE can be more

165 straightforwardly estimated from field measurements across various spatiotemporal scales,

166 including leaf gas exchange (daily to weekly at the leaf level), dendrochronology

167 (seasonal/annual at the tree level), and eddy covariance (hourly at the stand level) (more

168 discussion on iWUE at different scales is available from Beer et al., 2009 and Yi et al., 2019).

169 Notably, the inference of iWUE from tree-ring analyses provides an avenue for understanding

170 historical variations in iWUE and, potentially, mWUE. While iWUE has a mathematically

171 simpler form and thus facilitates modeling its response to water stress, the complex mathematical

172 expression of mWUE poses challenges in generalizing its variability at a sub-daily timescale. By

173 elucidating the correlation between iWUE and mWUE, we can gain insights into the response of

174 mWUE to water stress. Additionally, through site comparisons, we further explore whether there

175 is an emerging pattern in the correlation between iWUE and mWUE across different vegetation

176 types and aridity levels.

177

178   Table 1. A glossary of terms related to water-use efficiency.

Term or symbol	Definition
A	Carbon assimilation rate
AI	Aridity index: the ratio of annual precipitation to annual potential evapotranspiration
c_a	Atmospheric CO_2 concentration
E	Transpiration rate
ET	Evapotranspiration rate
g_0	Intercept parameter in Ball-Berry model (represents minimum leaf conductance)
g_1	Slope parameter in Ball-Berry model (represents marginal water-use efficiency, mWUE)
g_s	Stomatal conductance
G_s	Surface conductance
GPP	Gross primary productivity
iWUE	Intrinsic water-use efficiency; leaf-level water-use efficiency ($= A / g_s$)
IWUE	Inherent water-use efficiency; a proxy of intrinsic water-use efficiency at the ecosystem level ($= GPP / ET \times VPD / P_a$, Beer et al., 2009)
$m*$	The slope of the linear relationship between $IWUE^{-1}$ and mWUE
mWUE	Marginal water-use efficiency, the ratio of a change in E to a change in A ($= \partial E / \partial A$)
P_a	Atmospheric pressure
VPD	Vapor pressure deficit

179

2. Materials and Methods

2.1. FLUXNET data

182   We obtained half-hourly measurements of carbon and energy fluxes, along with ancillary

183   environmental data, from 115 flux towers across FLUXNET sites. These data were collected

184   using the FLUXNET 2015 Tier 1 database (Table S1) (Pastorello et al., 2020). Eddy covariance

185   records, which have the benefit of providing continuous meteorological and gas exchange data at

186   the high temporal resolution, are very well suited for investigating the relationship between gas

187   exchange dynamics, mWUE, and VPD at the ecosystem scale.

188   We selected the study sites from six vegetation types (grassland, cropland, shrubland,

189   savanna, broadleaf forest, and needleleaf forest, based on the International Geosphere-Biosphere

190   Programme (IGBP) land cover classification system; Loveland & Belward, 1997) based on the

191   data availability for the variables required for the analysis. For reliable and clear mWUE

192   analysis, we only included the sites that had at least three years of data and a strong iWUE-VPD

193   correlation. Specifically, we selected the sites that had a coefficient of determination (R^2) > 0.8

194   with any of the three model fits—linear, quadratic, or Michaelis-Menten, which was the case for

195   more than 70% of the sites over three years of data (refer to section 2.4 for more information

196   about the model fits). In addition, we only used the data where net ecosystem exchange (NEE),

197   latent heat flux (LE), and sensible heat flux (H) were either original measurements (quality

198   control flag = 0) or gap-filled data of good quality (quality control flag = 1) to ensure data

199   quality and make the most of the data. We only used daytime data when net radiation was greater

200   than 0 W m^{-2} without precipitation. While we acknowledge the potential benefits of excluding

201   more days after rainfall (e.g., Lin et al., 2015), we believe that omitting only the precipitation

202   days is sufficient for our analysis. This is because iWUE had low variability under humid

203   conditions, as evidenced by the low standard deviations of IWUE under low VPD levels in

204   Figure 2. Additionally, we implemented a procedure to remove outliers in soil water content and

205   relative humidity as described in the following paragraph, which would help mitigate the impact

206   of periods after rainy days on our analysis.

207   We limited our analysis to the growing season, where daily GPP was larger than 10% of

208   the 95th percentiles of daily GPP for each site with > 5°C air temperature. We used the GPP

209 partitioned based on the standard daytime method (variable name: GPP_DT_VUT_REF, Lasslop

210 et al., 2010). Additional filtering criteria were applied for some key variables: atmospheric CO_2

211 concentration between 350 ppm and 420 ppm, friction velocity (u^*) greater than 0.1 m s^{-1}, and

212 canopy conductance calculated by Penman-Monteith equation (Monteith, 1965) greater than 0.05

213 mol m^{-2} s^{-1}. Lastly, we removed outliers of the environmental drivers and biological variables

214 (i.e., air temperature, relative humidity, atmospheric CO_2 concentration, latent heat flux, wind

215 speed, VPD, atmospheric pressure, friction velocity, net radiation, soil water content, canopy

216 conductance, iWUE, and mWUE) by excluding data that were below the 5th or above the 95th

217 percentiles of each variable. Note that the purpose of data filtering was to remove exceptionally

218 low or high values of the variables, which we consider outliers. Our goal was to ensure that the

219 results, especially the variability of mWUE, were not unduly influenced by these outliers. We

220 carefully examined the histograms for the variables for each site to minimize data reduction

221 while retaining useful information.

222

223 **2.2. Two different approaches describing mWUE**

224   We used two different approaches for describing the mWUE: two optimization-theory-

225 driven mWUE, the solution of "$\partial E / \partial A$" suggested by Katul et al. (2010) and the "g_1" parameter

226 proposed by Medlyn et al. (2012). The difference between the optimization-theory-driven

227 mWUE is based on their interpretation of stomatal optimization. Katul et al. (2010) assumed that

228 stomata are optimizing for photosynthesis limited by Rubisco activity (i.e., carbon-limited), and

229 plant stomatal optimality is subject to change (i.e., mWUE is not constant). On the other hand,

230 Medlyn et al. (2012) assumed that stomata are optimized for photosynthesis limited by Ribulose-

231 1,5-bisphosphate (RuBP) regeneration (i.e., light-limited). In either case, the optimization

232 objective should result in constant mWUE values at short timescales—Katul et al. (2010)

233 suggested approximately 10 minutes, whereas Medlyn et al. (2012) suggested daily or longer—

234 although it may change at longer timescales as hydrologic conditions evolve.

235 Following Katul et al. (2010), the $\partial E/\partial A$ emerges from an optimality condition

236 determined with a linearized variant of the Farquhar et al. (1980b) photosynthesis model, defined

237 as:

$$\frac{\partial E}{\partial A} = 1.6 \, \text{VPD} \, c_a \left(\frac{A}{g_s}\right)^{-2} = \frac{1.6 \, \text{VPD} \, c_a}{\text{iWUE}^2} \qquad (3)$$

238

239 where iWUE is defined as a ratio of A to g_s at the leaf-scale (Beer et al., 2009).

240 The other perspective on optimality proposed by Medlyn et al. (2012) takes an analogous

241 form to an empirical model proposed by Leuning (1995) (Eq. 2):

$$g_s \approx g_0 + 1.6 \left(1 + \frac{g_1}{\sqrt{\text{VPD}}}\right) \frac{A}{c_a} \qquad (4)$$

242

243 This approach indicates that the parameter g_1 represents a slope between g_s and $A/c_a\sqrt{\text{VPD}}$ and

244 is proportional to $\sqrt{\partial E/\partial A}$ (Lin et al., 2015; Medlyn et al., 2012). Therefore, to facilitate

245 comparison between the two approaches, we compare $\partial E/\partial A$ with squared g_1 (i.e., g_1^2)

246 throughout the results. Eq. 4 was rearranged with an assumption that g_0, which represents

247 cuticular conductance to water vapor, is negligible (but refer to Manzoni et al. (2011) and

248 Lanning et al. (2020) for discussion of the role of cuticle conductance under drier conditions):

$$g_1 = \left(\frac{g_s \, c_a}{1.6 \, A} - 1\right)\sqrt{\text{VPD}} = \left(\frac{c_a}{1.6 \, \text{iWUE}} - 1\right)\sqrt{\text{VPD}} \qquad (5)$$

249

250 Consequently, two different mWUE parameters, $\partial E/\partial A$ (mol $H_2O \cdot$ kPa $\cdot$ mol^{-1} of dry air) and g_1

251 (mol $H_2O \cdot$ kPa$^{0.5} \cdot$ mol^{-1} of dry air), were expressed as functions of iWUE, c_a, and VPD.

252 Assuming c_a is relatively stable over a short period, we focus on how iWUE (as a biological

253 factor) and VPD (as an indicator of water stress governing plant response at a short temporal

254 scale, e.g., sub-daily) affect both mWUE parameters (more details discussed in section 2.5). We

12

255   applied an approximation of iWUE at the ecosystem level, inherent WUE (IWUE), defined by

256   Beer et al. (2009). IWUE (μmol C mol^{-1} H$_2$O) was particularly suitable for our study because

257   IWUE can be calculated from the measurements of carbon and water fluxes by eddy covariance

258   technique and ancillary meteorological data, i.e., gross primary productivity (GPP; μmol m^{-2} s^{-1})

259   from net ecosystem exchange representing canopy-level carbon assimilation, evapotranspiration

260   rate (ET, mol m^{-2} s^{-1}) from latent heat flux, VPD under the assumption of equal temperatures of

261   leaves and atmosphere, and atmospheric pressure (P_a, kPa):

262
$$IWUE = \frac{GPP \cdot VPD}{ET \cdot P_a} \qquad (6)$$

263

264   Several important assumptions for the definition of IWUE include (1) small and invariant soil

265   evaporation (E) compared to plant transpiration (T) over the course of the day (hence $\Delta ET \sim \Delta T$)

266   especially during days without rainfall (conditions we used for our analysis), (2) thermal

267   equilibrium between leaf and air, which influences VPD, and (3) disregarding of aerodynamic

268   resistance through the boundary layer that can change depending on the vegetation structure

269   (refer to Beer et al. (2009) for more discussion about IWUE as a proxy of ecosystem-level

270   iWUE). We confirmed the robustness of IWUE as a proxy of iWUE at the ecosystem level by

271   comparing it with a few other definitions of iWUE (the comparison results are available in the

272   Supporting Information; Figs. S1 & S2). Note that IWUE and mWUE were computed using half-

273   hourly FLUXNET data; hence, their variabilities discussed here represent plant physiological

274   response at a sub-hourly scale.

275

276   **2.3. Sensitivity of mWUE parameters to moisture condition**

277   Variations of mWUE parameters in response to moisture conditions (i.e., atmospheric

278   water demand and site-level aridity) were evaluated at the individual site level and across sites.

279   For the individual sites, mWUE parameters were partitioned into discrete bins spanning a range

280   of VPD. To avoid biases from unevenly distributed data points across the range of VPD (i.e.,

281   sample sizes at low and high VPD are smaller than those for the intermediate level of VPD), data

282   binning was performed in a way that the sample sizes were evenly distributed into 30 bins across

283   the range of VPD at each site. Then, mWUE-VPD relationships were produced based on the

284   mean mWUE values generated for the different VPD bins.

285   To compare across the sites, the relationships between site-specific mWUE and aridity

286   index (AI) were evaluated (refer to Fig. S3 in the Supporting Information for AI at all the study

287   sites). AI was defined as the ratio of annual precipitation (P) to annual potential

288   evapotranspiration (PET) and averaged over the observation period for each site (UNEP, 1992):

289 $$AI = \frac{P}{PET} \qquad (7)$$

290   The annual PET was determined by summing up the half-hourly PET values over the course of a

291   year, using the United Nations Food and Agriculture Organization (FAO) Penman-Monteith

292   method as outlined by Allen et al. (1998):

293 $$PET = \frac{0.408\Delta(R_n - G) + \gamma \frac{900}{T_a + 273} u(e_s - e_a)}{\Delta + \gamma(1 + 0.34u)} \qquad (8)$$

294   where Δ is the slope of vapor pressure curve (kPa °C^{-1}), R_n is the net radiation (MJ m^{-2} hr^{-1}), G is

295   the soil heat flux density (MJ m^{-2} hr^{-1}), γ is the psychrometric constant (kPa °C^{-1}), T_a is the air

296   temperature (°C), u is the wind speed (m s^{-1}), e_s is the saturation vapor pressure (kPa), and e_a is

297   the actual vapor pressure (kPa). The estimation of AI is sensitive to gaps in precipitation data.

298   Therefore, we used long-term mean annual precipitation provided on the site information page at

14

299   the FLUXNET website (https://fluxnet.org/sites/site-list-and-pages/) rather than calculating mean

300   annual precipitation from the FLUXNET2015 dataset. For the sites where annual precipitation

301   records were not provided, the high-frequency precipitation record in the FLUXNET2015 dataset

302   was used.

303

304   **2.4. Assessing the relationship between mWUE and IWUE**

305   As a first step to conceptually understand the relationship between mWUE and IWUE,

306   the relationship between IWUE and VPD was modeled by three hypothetical functions—linear,

307   quadratic, and the Michaelis-Menten functions—based on the observations across the sites. The

308   quadratic model of IWUE-VPD (hereafter $IWUE_Q$) depicts the case where IWUE increases with

309   VPD until it reaches a maximum and then decreases afterward. In other words, when VPD is

310   low, increasing IWUE with increasing VPD reflects a faster decrease of g_s than A (due to the

311   high intercellular CO_2 concentration, c_i), whereas decreasing IWUE with increasing VPD at high

312   VPD reflects a faster decrease of A than g_s (low g_s at high VPD reduces c_i and eventually causes

313   the steep decline of A). The linear model (hereafter $IWUE_L$), on the other hand, represents a

314   simplified IWUE-VPD relationship where IWUE would keep increasing with rising VPD

315   assuming IWUE is only limited by g_s but not by photosynthetic capacity. The Michaelis-Menten

316   function (hereafter $IWUE_M$) represents the saturating IWUE under high VPD but does not

317   account for IWUE reduction. Thus, the linear and quadratic functions are considered plausible

318   "end members" describing the actual response of IWUE to VPD, while the Michaelis-Menten

319   function is a more intermediate case. Mathematically, the $IWUE_L$, $IWUE_M$, and $IWUE_Q$ take the

320   forms:

321 $$IWUE_L = m\,VPD + n \qquad (9)$$

$$IWUE_M = \frac{IWUE_{max} \cdot VPD}{k + VPD} \qquad (10)$$

$$IWUE_Q = -a\,(VPD - b)^2 + c \qquad (11)$$

where m is the slope of $IWUE_L$, n is $IWUE_L$ at VPD = 0, $IWUE_{max}$ is the maximum potential

IWUE, k is the VPD at which IWUE proceeds at half $IWUE_{max}$, a represents the curvature of

$IWUE_Q$, b is the vertex, c is the maximum $IWUE_Q$ at the vertex.

The expected dynamics of mWUE across the FLUXNET sites in response to changing

VPD were simulated based on an empirically driven IWUE-VPD model to understand how the

mWUE metrics would respond to changing VPD and IWUE. To generate possible patterns of

mWUE-VPD, the range of coefficients in the IWUE models was determined empirically from

the data across the sites. To facilitate interpretation, the patterns were simulated by changing the

curvature of the quadratic equation (Eq. 11), assuming the intercept is equal to zero. For the

simulation of mWUE, a constant c_a was applied by calculating its average across the sites to

focus on the interactions among VPD, IWUE, and mWUE (Eqs. 3 & 5).

Lastly, we investigated how IWUE (as a biological factor) and aridity index (as an

environmental driver) influence the variability of mWUE. Based on the Eqs. 3 and 5, we

hypothesized that a simple relationship between mWUE and the inverse of IWUE ($IWUE^{-1}$)

might emerge and would be affected by changing moisture conditions. Therefore, we identified a

relationship between mWUE and $IWUE^{-1}$ for each study site and examined whether the

relationship can be generalized across the sites based on the site-specific aridity index.

3. Results

3.1. Empirical response of IWUE to changing VPD or AI

344   To test the robustness of IWUE as a proxy of intrinsic water-use efficiency at the

345   ecosystem level, we first compared the two different definitions of intrinsic water-use

346   efficiencies at stand level, GPP divided by surface conductance (G_s) (i.e., iWUE = GPP/G_s) and

347   inherent WUE (i.e., IWUE = GPP/ET×VPD/P_a). The two WUE definitions were linearly

348   correlated across the study sites (Fig. 1), and most sites had R^2 values larger than 0.95 (Fig. 1b),

349   indicating the robustness of IWUE as a proxy of intrinsic water-use efficiency at the ecosystem

350   level (refer to the Supporting Information for an additional comparison of multiple definitions of

351   intrinsic water-use efficiency; Figs. S1 & S2). We also performed the entire analysis using these

352   two WUE definitions and observed similar results, which led to the same conclusion. Therefore,

353   we only show the results from using IWUE hereafter.

354

355

17
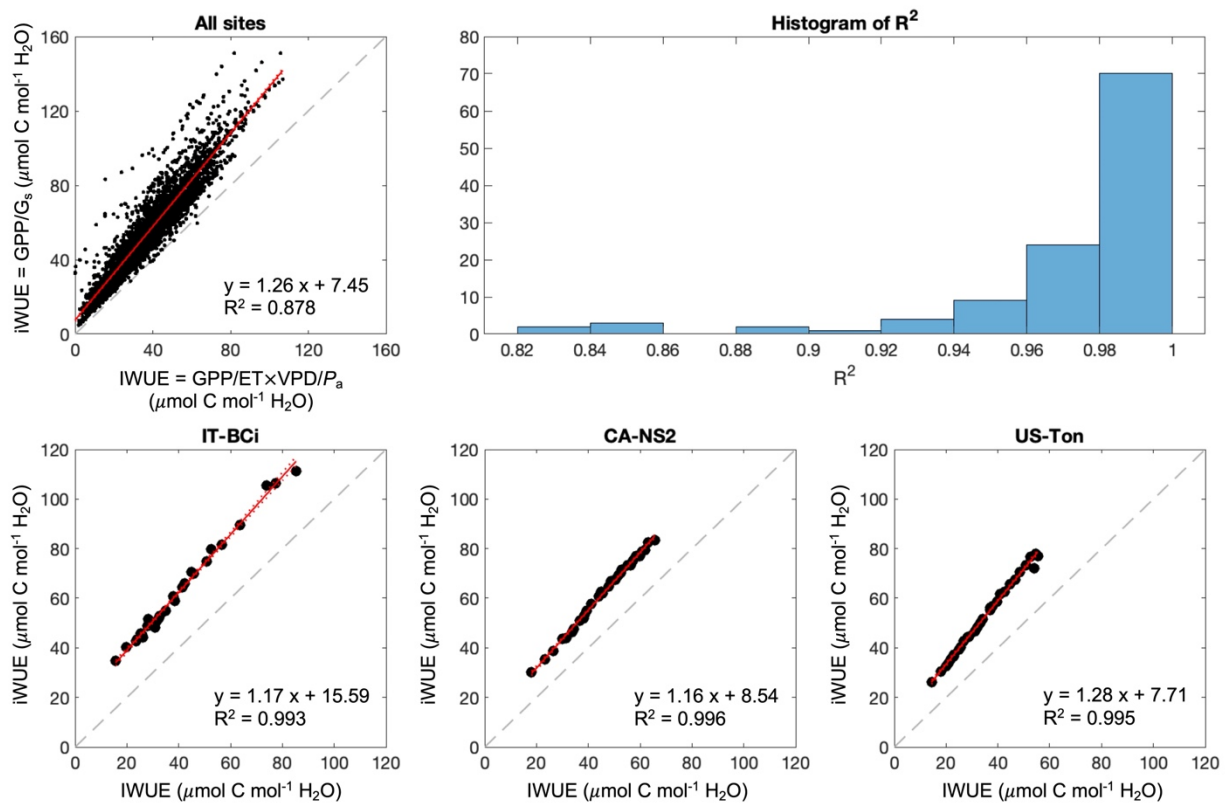
356 **Figure 1.** Comparison of two different definitions of water-use efficiencies at all sites (a) and at

357 three sample sites (c, d, e): inherent water-use efficiency at the ecosystem level, IWUE (=

358 GPP/ET×VPD/P_a), and intrinsic water-use efficiency at the ecosystem level, iWUE (= GPP/G_s).

359 Refer to Beer et al. (2009) for the comparison of different definitions of water-use efficiencies at

360 leaf and ecosystem-level. Individual dots in panels a, c, d, and e indicate WUE partitioned into

361 discrete bins spanning a range of VPD. Solid red lines indicate significant linear regressions (P <

362 0.05), and dashed red lines indicate 95% confidence interval. Dashed gray lines represent 1:1

363 lines. Panel b shows the histogram of coefficients of determination (R^2) of the linear fits between

364 IWUE and iWUE across the study sites.

365

366   In most cases, the Michaelis-Menten model and the quadratic model explained empirical

367 IWUE patterns across the range of VPD better than the linear model (Fig. 2 and Fig. S3 in the

368 Supporting Information). Specifically, the Michaelis-Menten model worked better for the sites

369 where the increase of IWUE plateaued at high VPD, and the quadratic model worked better for

370 the sites where IWUE started decreasing at very high VPD. On the other hand, the linear model

371 often overestimated IWUE at low and high VPD, except the sites where IWUE-VPD was highly

372 linear.

373
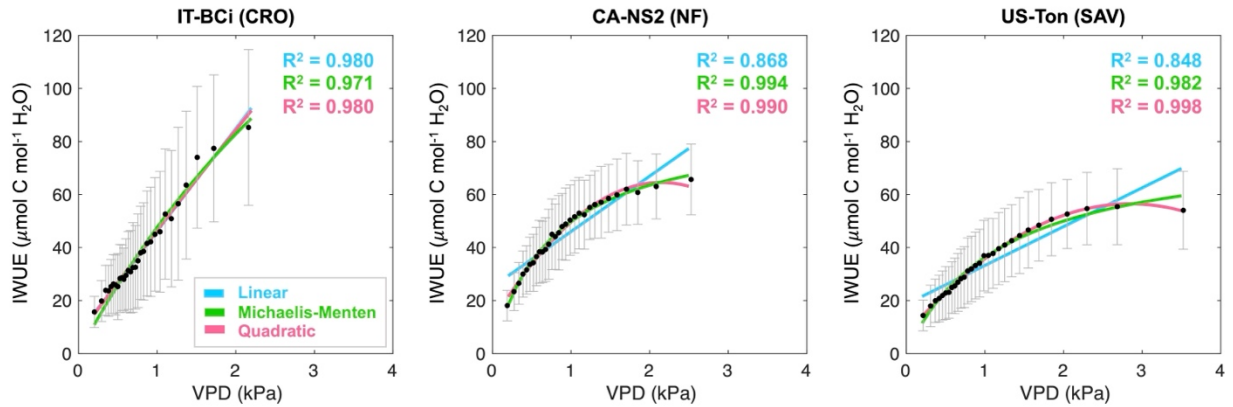
Figure 2. Examples of empirical (black dots) and modeled (linear: blue, Michaelis-Menten: green, quadratic: red) responses of inherent water-use efficiency (IWUE) to changing vapor pressure deficit (VPD). The examples include three sites best represented by the linear model (IT-BCi, cropland), the Michaelis-Menten function (CA-NS2, needleleaf forest), and the quadratic model (US-Ton, savanna), respectively. Each error bar (light gray) represents the standard deviation of IWUE for each VPD bin (95% confidence). Refer to Fig. S4 in the Supporting Information for the IWUE-VPD relationships of all the study sites ($n = 115$).

When the site-specific IWUE-VPD slope values derived from the linear model (i.e., m in Eq. 9) were combined, we found increasing m with rising aridity index ($P < 0.001$, Fig. 3a). However, site-level aridity did not influence the intercept of IWUE-VPD relationship ($P > 0.05$, not shown here). When the sites were divided by their vegetation types, m increased with a rising aridity index in all vegetation types. However, the trend was only significant in grasslands, croplands, and shrublands ($P < 0.05$, Fig. 3).
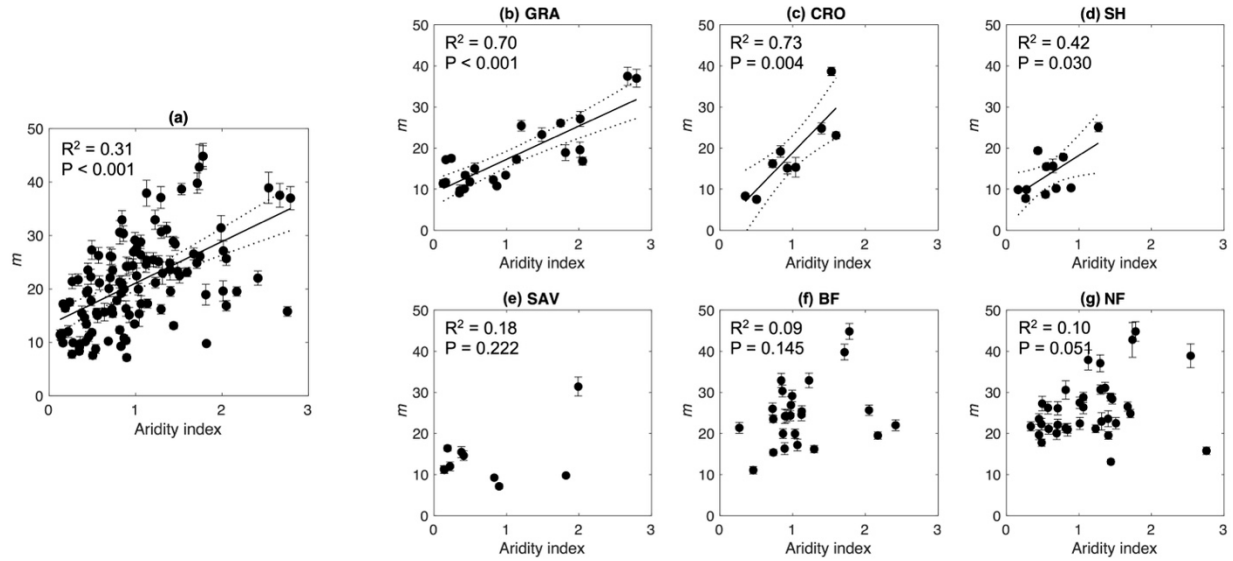
Figure 3. Relationship between the site-level aridity index and the regression slope of IWUE-VPD from individual sites (i.e., m in Eq. 9). Panel a shows the relationship when all sites were consolidated. The relationship is also illustrated separately for six different vegetation types in panels b to g (GRA: grassland, CRO: cropland, SH: shrubland, SAV: savanna, BF: broadleaf forest, NF: needleleaf forest). Each circle represents m from an individual site. Error bars represent standard errors of linear regressions. Solid lines indicate significant linear relationships ($P < 0.05$) and dashed lines indicate 95% confidence intervals.

3.2. Response of mWUE to changing VPD

Both of the mWUE indices, $\partial E / \partial A$ and squared g_1 (g_1^2), showed a very similar response to changing VPD and indicated that the directional change of mWUE can be interpreted differently depending on the pattern of IWUE-VPD (Fig. 4). When the iWUE-VPD relationship is strongly linear, mWUE decreased exponentially and became less variable as VPD increased (Brighter curves in Figs. 4b & 4c). However, as the iWUE-VPD relationship became more non-
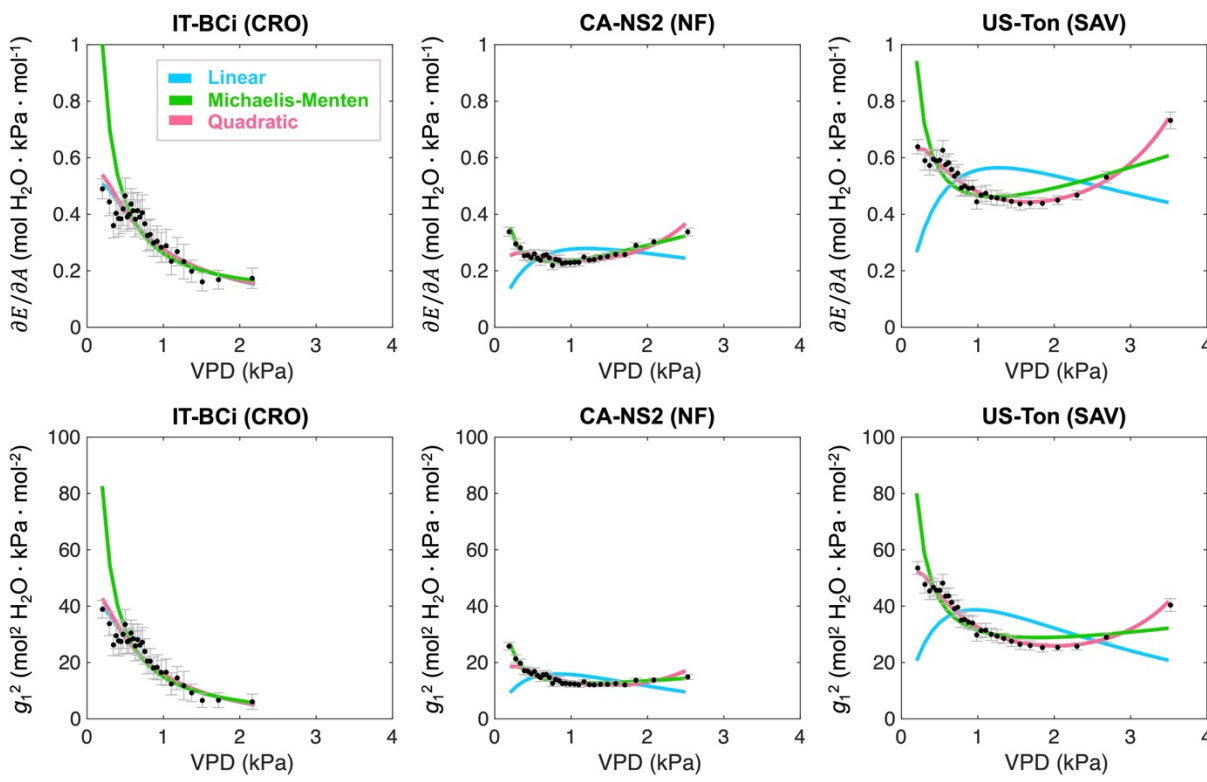
405 linear, mWUE declined at lower VPD and then increased at higher VPD (i.e., concave-up),

406 rendering the mWUE-VPD relationship non-monotonic (darker curves in Figs. 4b & 4c).

407
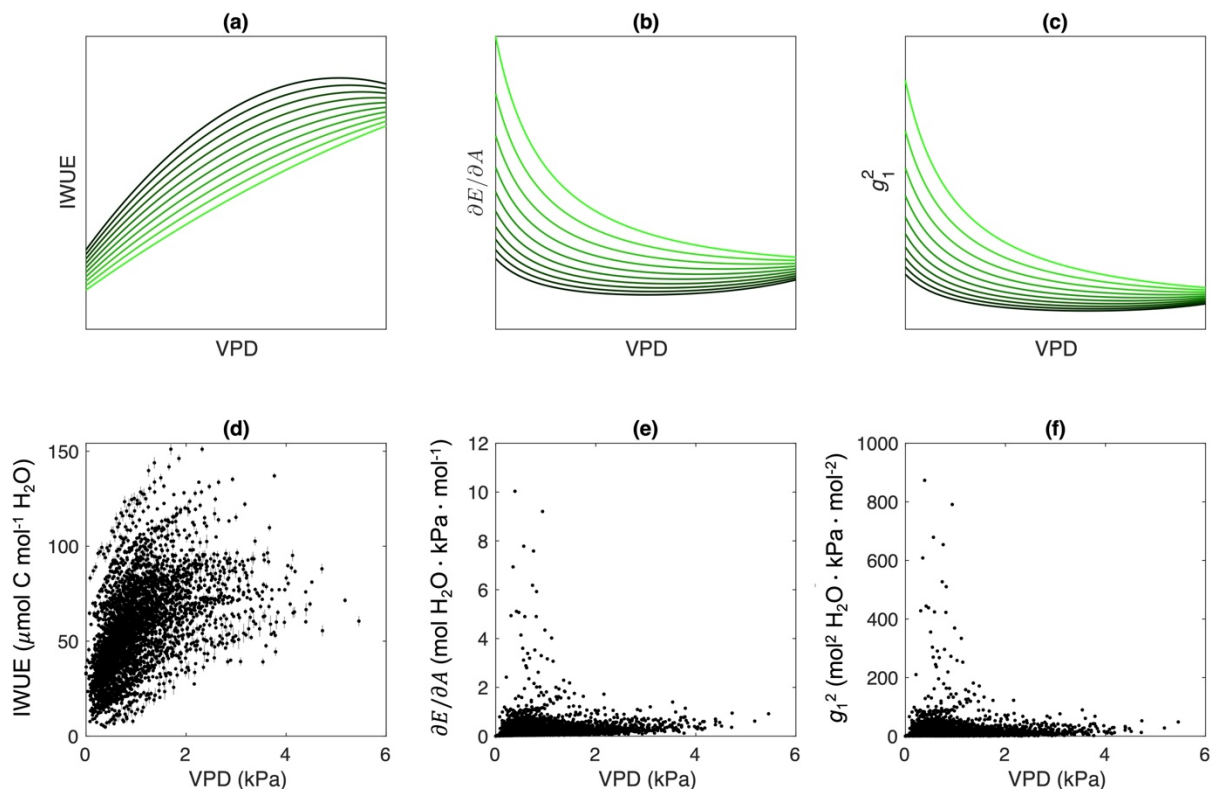
409 **Figure 4.** Hypothetical models of IWUE-VPD relationship (a), simulated $\partial E/\partial A$-VPD (b) and

410 g_1^2-VPD (c) relationships based on typical cases, and their corresponding patterns illustrated

411 using observations from all study sites (d, e, and f). The mWUE curves are the results of using

412 the IWUE-VPD relationships of the corresponding colors. Note that IWUE-VPD relationships

413 become more linear with lighter colors.

414

415   The simulated patterns of mWUE-VPD agreed well with the patterns from the empirical

416 observation when the appropriate function for the IWUE-VPD relationship was applied. We

417 show mWUE-VPD relationships from three study sites as examples (Fig. 5), of which IWUE-

21

418   VPD was represented best by linear, the Michaelis-Menten, and quadratic functions, respectively

419   (refer to Fig. 2 for their corresponding IWUE-VPD relationships. Also, refer to Fig. S5 in the

420   Supporting Information for the results of all study sites). As indicated by the simulation, the site

421   with highly linear IWUE-VPD (IT-BCi) showed exponentially decreasing mWUE with rising

422   VPD. In contrast, the other two sites with highly non-linear IWUE-VPD relationships had a

423   concave-up pattern of mWUE-VPD. Notably, the mWUE-VPD relationship generated using a

424   less optimal IWUE-VPD model can differ substantially from the empirical pattern. For example,

425   application of linear IWUE-VPD function to the CA-NS2 and US-Ton, the sites represented best

426   by the Michaelis-Menten and quadratic functions, respectively, generated concave-down

427   mWUE-VPD pattern that is opposite to the actual pattern (Fig. 5). The disagreements between

428   models and observations increased as VPD approached very high and very low extremes.

429

430

441

442   　　The variability of mWUE to changing VPD was substantial in most cases (Fig. 6). Out of

443   the total of 115 study sites, the percent increase of $\partial E/\partial A$ (i.e., growth in $\partial E/\partial A$ from the

444   lowest to the largest value at a site) was larger than 50% in 43 sites, and larger than 100% in 22

445   sites. Note that the reported percent increase was determined by excluding the upper and lower

446   10% of values. This step was taken to prevent exaggeration caused by extremely high $\partial E/\partial A$ at

447   low VPD, which is commonly observed across the study sites (refer to Figure S5 in the

448   Supporting Information for the variability of $\partial E/\partial A$ with VPD at all the study sites). As a result,

449   the reported percent increase represents a conservative estimate overall.

450

23
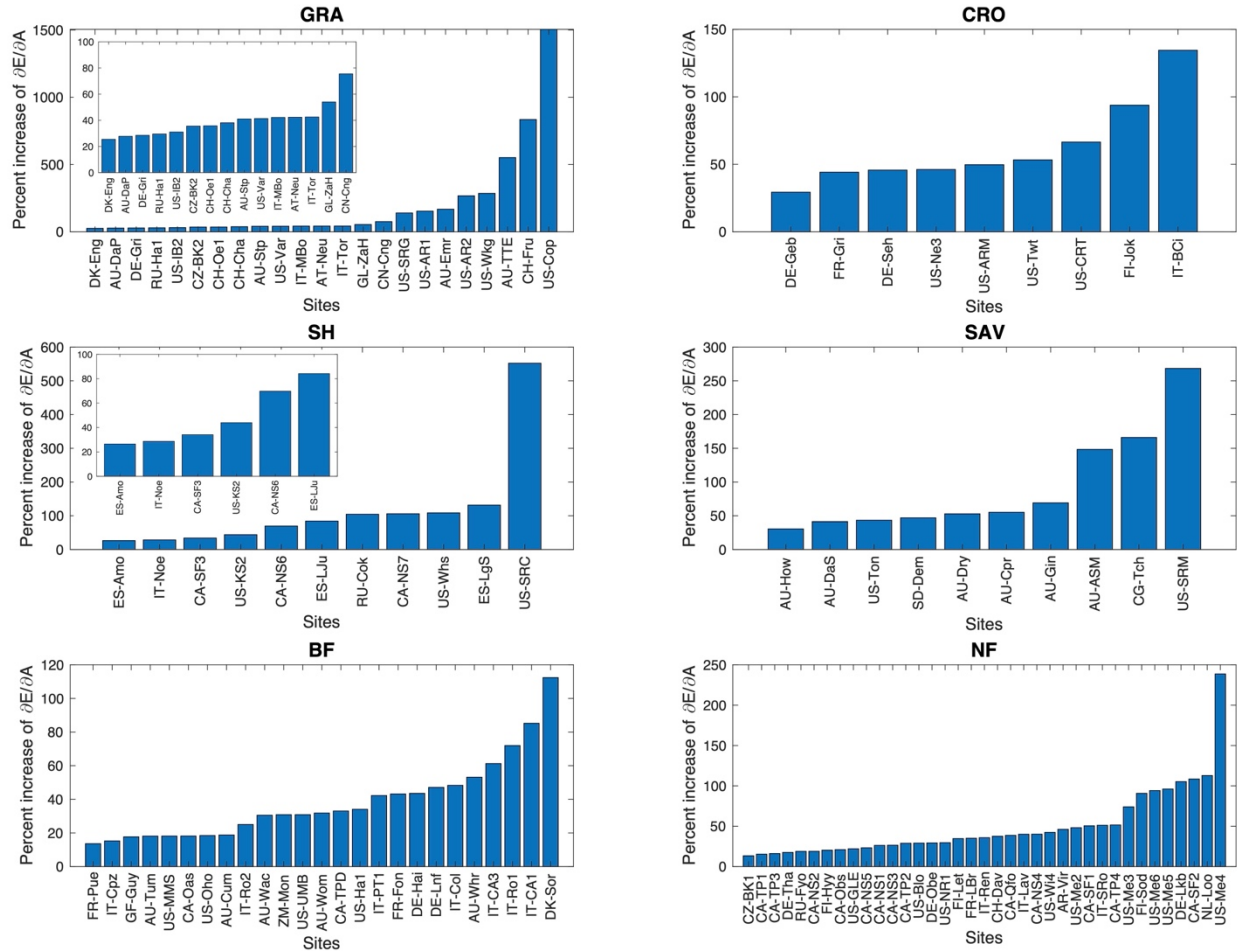
Figure 6. Sorted percent increase of $\partial E/\partial A$ (from the lowest $\partial E/\partial A$) (GRA: grassland, CRO: cropland, SH: shrubland, SAV: savanna, BF: broadleaf forest, NF: needleleaf forest). Embedded plots in GRA and SH are zoomed in for those sites where percent increases are lower than 100%. Note that the percent increases were calculated after removing values of the highest 10% and lowest 10% to avoid exaggeration due to very high $\partial E/\partial A$ at low VPD at some sites. Therefore, the reported percent increase values are conservative estimates for most sites.

3.3. Correlation between mWUE and IWUE

Although the trend of mWUE-VPD seems hard to generalize, the simulated mWUE had a clear linear relationship with IWUE^{-1} for the majority of IWUE's range regardless of the linearity

462 of the IWUE-VPD relationship except when IWUE is very high (i.e., under high VPD, Fig. 7).

463 Although limited to a small portion of the entire range, a sharp directional change in the variation

464 of mWUE was near a point where IWUE^{-1} was smallest, and strong linearities between mWUE

465 and IWUE^{-1} were found before and after the transitional point. Substantial hysteresis became

466 more evident as the IWUE-VPD pattern became more curved (darker curves in Fig. 4).

467

468
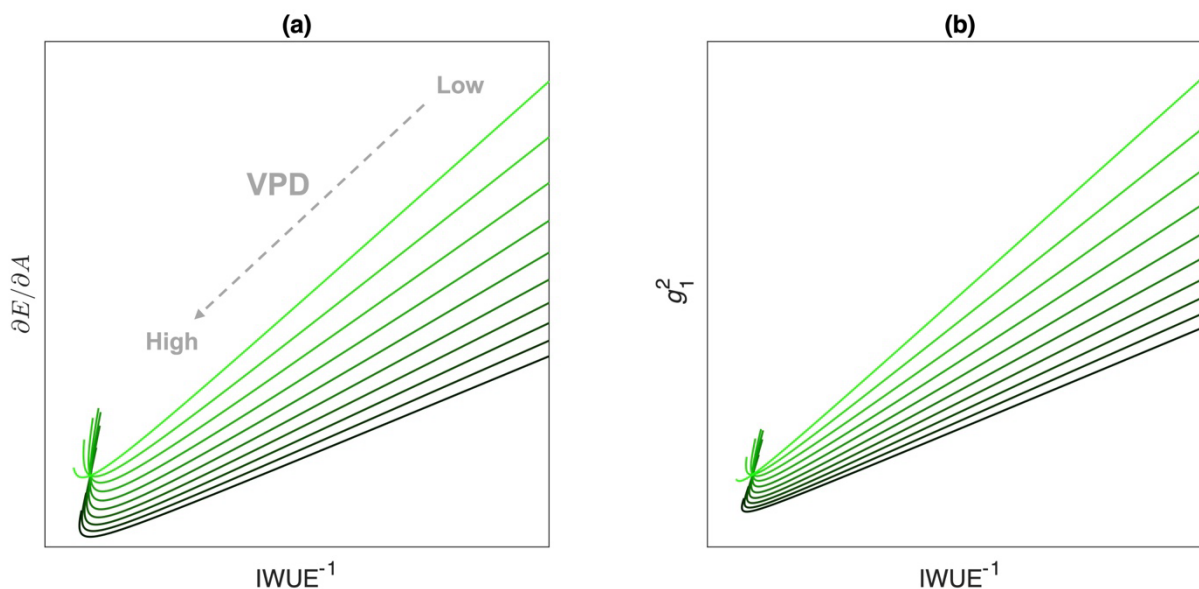
Figure 7. Simulated relationship between mWUE metrics ($\partial E / \partial A$ and g_1^2) and IWUE^{-1} (based
on the hypothetical IWUE-VPD model in Fig. 4). The colors of the curves correspond to those
used in Fig. 4: IWUE-VPD relationships become more linear with lighter colors. Dashed arrows
in panel a represent the directional change of VPD from low to high VPD.

473

474 As predicted by the simulated mWUE-IWUE^{-1} relationships (Fig. 7), the empirical

475 mWUE-IWUE^{-1} relationship was strongly linear ($P < 0.001$ at all sites, Fig. 8). A sign of

476 hysteresis was noticeable for the site that showed decreasing iWUE under very high VPD (US-

477   Ton, refer to Fig. 2 for its IWUE-VPD relationship). In contrast, hysteresis was less evident at

478   the other sites. When the relationship was drawn by grouping data by different levels of IWUE

479   (black dots in Fig. 8), hysteresis was not observed, and the mWUE-IWUE[-1] relationship was

480   strongly linear.

481

482
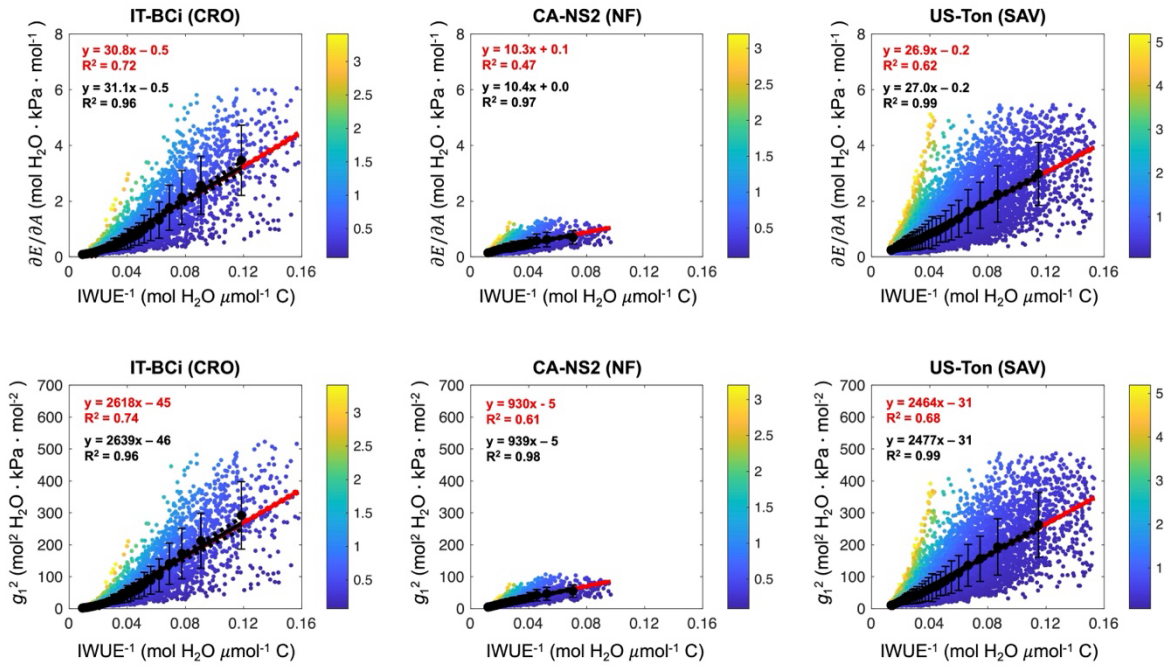
Figure 8. Examples of empirical relationship between mWUE metrics ($\partial E/\partial A$ and $g_1{}^2$) and IWUE^{-1}. The examples include three sites best represented by the linear IWUE-VPD model (IT-BCi, cropland), the Michaelis-Menten function (CA-NS2, needleleaf forest), and the quadratic model (US-Ton, savanna), respectively. Refer to Fig. 2 for the IWUE-VPD relationships at the corresponding sites. Colorful dots represent hourly data points shaded based on the level of VPD (refer to color bars for the scale of VPD). Black dots represent data binned by IWUE^{-1}: Data binning was performed to distribute sample sizes evenly across bins (~30 samples per bin). Error bars represent standard deviations. The red and black solid lines indicate linear fits for hourly and binned data, respectively. Dashed red lines represent confidence intervals for the slopes of linear regressions. Note that red and black linear regressions and their confidence intervals overlap. Refer to Fig. S6 in the Supporting Information for the $\partial E/\partial A$ - IWUE^{-1} relationships at the 115 study sites.

We investigated whether the relationship between mWUE and IWUE^{-1} could be generalized across the sites based on the site-specific AI. Specifically, the linear IWUE^{-1}-mWUE slopes (hereafter *m**) from all study sites were merged, and their variability in response to changing AI was evaluated. We found a significant linear relationship between *m** and AI when both are scaled by $\log_{10}$ (P < 0.001, Fig. 9). The *m** was larger at the drier sites (i.e., sites of lower AI) than at the wetter sites (i.e., sites of larger AI). However, we did not find a significant relationship between the IWUE^{-1} – mWUE intercept and AI (P > 0.05, not shown here).
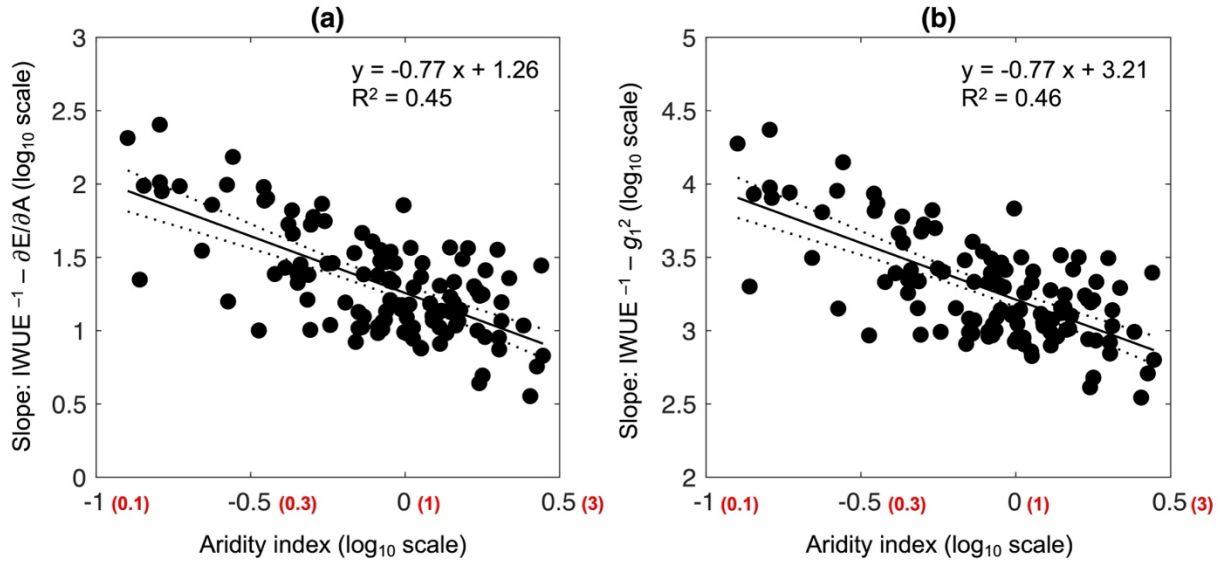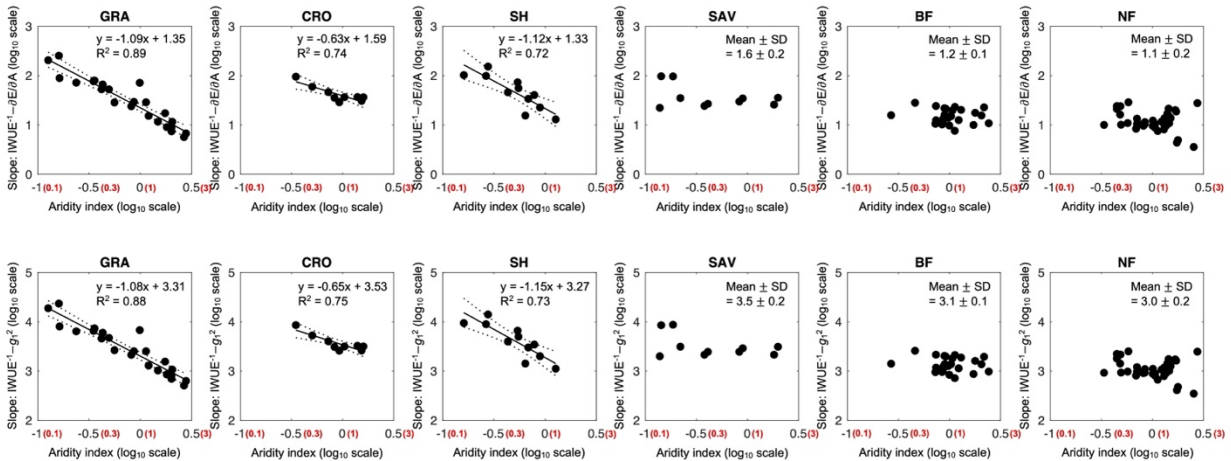
Figure 9. Relationships between IWUE^{-1}-mWUE slope and aridity index (= P/PET) derived from all the study sites ($n = 115$). Each circle represents the slope obtained from an individual site. Both the x and y axes are scaled by $\log_{10}$. The numbers in parentheses next to the x-axis tick labels represent the aridity indices before the log transformation. The solid lines indicate linear regressions, and the dashed lines indicate confidence intervals (95% confidence interval).

We further tested whether we could find the similar relationship when the sites were grouped by the vegetation type. We found decreasing m^* with rising AI in grasslands, croplands, and shrublands (P < 0.01, Fig. 10). On the other hand, m^* was relatively constant across the range of AI in savannas, deciduous broadleaf forests, and evergreen needleleaf forests (P > 0.05, Fig. 10).

Figure 10. Relationships between log-transformed $IWUE^{-1}$-mWUE slope and aridity index in different vegetation types (GRA: grassland, CRO: cropland, SH: shrubland, SAV: savanna, BF: broadleaf forest, NF: needleleaf forest). Each circle represents the log-transformed slope obtained from an individual site. The numbers in parentheses next to the x-axis tick labels represent the aridity indices before the log transformation. Solid lines indicate significant linear relationships ($P < 0.05$), and dashed lines indicate 95% confidence intervals.

4. Discussion

Stomatal optimization theory, which originated with the work of Cowan and Farquhar (1977), has experienced a recent surge in popularity as the vegetation modeling community continually seeks ways to inject more theoretical rigor into Earth system models (Anderegg et al., 2018; Bassiouni & Vico, 2021; Bonan et al., 2014; Feng et al., 2022; Katul et al., 2010; Katul et al., 2009; Lin et al., 2018; Lin et al., 2015; Lu et al., 2020; Lu et al., 2016; Medlyn et al., 2012, 2017; Novick et al., 2016b; Sabot et al., 2022; Sperry et al., 2017; Wolf et al., 2016). The marginal water-use efficiency (mWUE) is a key parameter in this type of model, but we still need a clear understanding of how mWUE is regulated biologically and environmentally. Lin et

al. (2018) previously suggested suboptimal mWUE in response to VPD at a sub-daily scale by

estimating site-specific, best-fitted exponent for VPD based on the variation model of optimality

theory (Medlyn model), which inspired our study. In comparison, our study is unique in

analyzing the dynamics of mWUE observed at the half-hourly timescale in response to changing

VPD owing to the long-term continuous carbon and water flux data from the network of eddy

covariance towers.

Another motivation for our study was the conflicting arguments over the dynamics of

mWUE in response to water stress. Although mWUE is in general considered to be nearly

constant during a day under stable soil moisture conditions (Berninger & Hari, 1993; Fites &

Teskey, 1988; Hall & Schulze, 1980; Hari et al., 2000), several studies showed that mWUE

changed with different levels of water stress. For example, theoretical considerations indicate a

monotonic decrease of mWUE with higher water stress when the stochasticity of rainfall depths

is neglected (Cowan, 1982; Makela et al., 1996), although some empirical estimates showed that

mWUE increases under severe water stress (Farquhar et al., 1980b; Grieu et al., 1988). On the

other hand, Manzoni et al. (2011) performed a meta-analysis of 50 species to estimate mWUE

from gas exchange observations along gradients of soil moisture and showed that mWUE

decreases under mild water stress but increases under severe water stress (note that they defined

$\lambda = \partial A/\partial E$, which is inverse of the definition used by Cowan & Farquhar (1977) and this

study).

4.1. Relationship between IWUE and VPD

Based on the two equations of stomatal optimization theory (Eqs. 3 & 5), we first

characterized the variability of mWUE based on the relationship between IWUE and VPD,

557   representing biological and environmental factors, respectively. We show that the variability of

558   IWUE needs to be modeled accurately to emulate the variability of mWUE in response to water

559   stress correctly. For example, as demonstrated in Fig. 5 (CA-NS2 & US-Ton), oversimplifying

560   the IWUE-VPD relationship by modeling it with a linear function can incorrectly interpret

561   mWUE variability.

562   The non-linear IWUE-VPD relationship is presumably driven by different rates of carbon

563   assimilation and water loss in response to changing VPD at an hourly scale, reflecting the

564   balance between stomatal and non-stomatal limitations to photosynthesis at the leaf level

565   (Farquhar, 1978; Jones, 2014). Under low to moderate VPD conditions, photosynthesis is less

566   sensitive to changing intercellular CO_2 concentration because stomatal conductance is high

567   enough to maintain the high intercellular CO_2 when VPD is low to moderate. Therefore, the

568   quantity of reduced water loss by stomatal closure (ET at an ecosystem level) outweighs the

569   quantity of reduced carbon assimilation (GPP at an ecosystem level) when VPD rises (i.e.,

570    $|\Delta GPP| < |\Delta ET|$), resulting in the increasing phase of IWUE. As VPD keeps increasing,

571   photosynthesis can be limited when the reduction of stomatal conductance under high VPD

572   conditions substantially reduces intercellular CO_2 concentration (i.e., $|\Delta GPP| \approx |\Delta ET|$),

573   resulting in the steady phase of IWUE. As VPD becomes excessively high, photosynthesis will

574   be further suppressed by high temperature (Yamori et al., 2014) and low leaf water potential

575   (Lawlor & Tezara, 2009) that are associated with dry conditions (i.e., $|\Delta A| > |\Delta g_s|$), leading to

576   the decreasing phase of IWUE.

577   Therefore, assuming a linear IWUE-VPD relationship may not only fail to emulate

578   observations but also oversimplify the physiological responses to water stress. Our analysis

579   recommends using the Michaelis-Menten function for most sites while utilizing a quadratic

31

580   function for sites exhibiting extreme cases where IWUE declines under high VPD conditions.

581   The Michaelis-Menten function can be beneficial to characterize the IWUE-VPD relationship

582   because the maximum potential IWUE and the rate of IWUE increase can be identified during

583   parameterization (Eq. 10). Although the quadratic function can emulate IWUE-VPD

584   relationships very well or performs even better than the Michaelis-Menten function in some

585   cases where IWUE decreases at high VPD, it is parameterized empirically and as a result, lacks

586   mechanistic information. Nevertheless, the quadratic function is preferable to the linear function.

587   It is also important to consider the definition of water-use efficiency for accuracy. We

588   used inherent water-use efficiency (IWUE) as a proxy of intrinsic water-use efficiency (iWUE)

589   at the ecosystem level as suggested by Beer et al. (2009), which can be estimated by GPP and ET

590   inferred from the flux tower observations. This approximation is particularly useful over a more

591   common ecosystem-level iWUE = GPP/G_s because IWUE requires fewer variables and is easier

592   to extrapolate to a larger scale. However, it is important to note that ET/VPD in the equation of

593   IWUE (Eq. 6) is a proxy of canopy conductance, assuming the canopy is well coupled to the

594   atmosphere, boundary layer resistance is small, and thermal equilibrium between leaf and air is

595   achieved (Beer et al., 2009). In other words, IWUE under non-equilibrium between canopies and

596   atmosphere can be overestimated due to the higher VPD than the vapor pressure gradient near

597   the canopy surface (i.e., the difference between intercellular vapor pressure (e_i) and atmospheric

598   vapor pressure (e_a), $e_i - e_a$). Difference between leaf and air temperature can also influence the e_i

599     $- e_a$; if leaf temperature is higher than air temperature (as it often is, e.g., Novick & Barnes,

600   2023; Yi et al., 2020), e_i will increase while e_a remains constant, resulting in larger $e_i - e_a$ than

601   measured VPD and consequently underestimate IWUE. Therefore, it is important to address this

602   potential bias to quantify iWUE accurately. According to our results, the correlation between the

603 two ecosystem-level iWUE proxies was strong at the site level (Fig. 1), implying that the choice

604 of ecosystem-level iWUE definition is unlikely to influence our interpretation of the iWUE and

605 mWUE variabilities substantially. Furthermore, our comparison of multiple definitions of iWUE

606 using a mechanistic model, CANVEG (refer to the Supporting Information for more details),

607 indicated that IWUE is a good proxy of leaf-level iWUE and meets the general assumptions to

608 address scaling issues. Thus, we conclude that eddy covariance observation of carbon and water

609 fluxes is suitable to model the variability of intrinsic water-use efficiency in response to

610 changing VPD.

611 Of note, the linear relationship between the slope of IWUE-VPD and aridity index (Fig.

612 4) was stronger in the ecosystems characterized by lower vegetation types (e.g., grasslands,

613 croplands, and shrubland). In contrast, ecosystems with higher vegetation (e.g., savannas,

614 broadleaf forests, and needleleaf forests) exhibited a weaker relationship. This observation

615 implies a potential link between water-use efficiency and the vertical structure of vegetation,

616 although the exact underlying mechanism remains uncertain.

617

618 **4.2. Modeling the variability of mWUE**

619 We compared two solutions of mWUE by Katul et al. (2010) ($\partial E / \partial A$) and Medlyn et al.

620 (2012) (g_1) developed based on different assumptions on stomatal optimality (carbon-limited

621 versus light-limited) for more robust conclusion. Despite the difference in the assumption, both

622 solutions yielded very similar results throughout our analysis, confirming that the optimality

623 assumption had little effect on evaluating the variability of mWUE in response to changing

624 moisture conditions.

625   We characterized the trend of mWUE by using VPD as an environmental driver (Figs. 4

626   & 5), where its variability in response to VPD was unique and not necessarily unidirectional,

627   thus making it hard to generalize with commonly available functions. Specifically, the variability

628   of mWUE was simpler and decreased exponentially with rising VPD when the IWUE-VPD

629   relationship was more linear, making it easy to model the mWUE-VPD relationship (Figs. 4 &

630   5). However, the variability of mWUE was not unidirectional when the IWUE-VPD relationship

631   was non-linear, as observed in most cases (Fig. S5 in the Supporting Information); high

632   variability in mWUE is usually observed at low- and high-ends of VPD. On the other hand, when

633   mWUE was calculated under conditions of moderate VPD level only, the variability of mWUE

634   can be overlooked and considered constant. This complex pattern signifies the importance of a

635   comprehensive view of IWUE and mWUE across the full potential range of VPD. Observation

636   under conditions of a partial range of environmental factors is common in many types of field

637   measurements that have coarser time resolution (hourly versus daily to weekly, e.g., eddy

638   covariance versus leaf gas exchange measurements) unless they are performed frequently over a

639   long period to cover non-typical conditions. We were able to estimate precise variability of

640   mWUE matching with the hypothetical models owing to the large amount of data

641   (FLUXNET2015) collected every half-hour over the long period throughout the network of flux

642   towers (total 1,036 site years with many sites offering data collected over more than a decade),

643   highlighting the value of long-term, continuous measurements. Overall, our result of the mWUE-

644   VPD relationship supports the results of Manzoni et al. (2011) among the various conflicting

645   results over the response of mWUE in response to water stress, which found decreasing mWUE

646   under mild water stress and increasing mWUE under severe water stress from a meta-analysis of

647   gas exchange observations.

34

648   As a solution to model unique patterns of mWUE, we attempt to address its variability

649   with information that can be obtained easily from various types of field measurements (e.g., eddy

650   covariance, gas exchange, and tree-ring cores) and modeled empirically—IWUE. The

651   relationship between mWUE and IWUE was inferred from the two equations of the optimization

652   theory (Eqs. 3 & 5). We found a strong linear correlation between $IWUE^{-1}$ and mWUE from both

653   empirical data (Fig. 8) and modeling exercise (Fig. 7). In other words, the variability of mWUE

654   in response to changing VPD can be characterized by (1) the function of IWUE-VPD

655   relationship and (2) the slope between $IWUE^{-1}$ and mWUE. The relationship between IWUE-

656   VPD is relatively simple and can be identified with various field measurements. This raises the

657   question of whether a simple way exists to identify the slope between $IWUE^{-1}$ and mWUE. By

658   synthesizing the $IWUE^{-1}$-mWUE slopes across the sites, we found that the IWUE-mWUE slope

659   is highly correlated with the site-specific AI that can be characterized for different vegetation

660   types (Fig. 9). The correlation is conceivable from the equations of mWUE (Eqs. 3 & 5). If, for

661   instance, Eq. 3 is rearranged,

662
$$\frac{\partial E / \partial A}{IWUE^{-2}} \propto VPD \qquad (12)$$

663   indicating that the slope between mWUE and the inverse of IWUE is proportional to VPD,

664   which is commensurate with AI at a site-level. The correlation between the $IWUE^{-1}$-mWUE

665   slope and the AI at a site level implies that the aridity index is a good surrogate for the site-

666   specific $IWUE^{-1}$-mWUE slope.

667   We further illustrated how the correlations between the $IWUE^{-1}$-mWUE slope (m^*) and

668   AI vary across vegetation types (Fig. 10). Among the vegetation types, GRA, CRO, and SH had

669   strong correlations between m^* and AI, which indicated that using different m^* depending on the

670   site-level dryness would be appropriate. On the other hand, the low variability of m^* observed in

35

671   SAV, BF, and NF indicates that constant m^* can generate a reasonably accurate mWUE-VPD

672   relationship regardless of the site-level dryness. Although the reasons for this difference are not

673   entirely clear, this empirical relationship can help more accurately model the variability of

674   mWUE in response to changing VPD across the sites and biomes. Growth in data availability

675   across the flux tower network helps ensure the coverage of the full potential range of

676   environmental factors. More data availability can be achieved by consistently collecting good-

677   quality data from existing study sites and establishing new sites in underrepresented areas.

678   Furthermore, additional data would also help the development of m^* in detail, for instance, based

679   on the plant water-use strategies, with the aid of conjoined field measurements such as water

680   potential (Ψ) of soil and plant.

681

682   **4.3. Implications for future research**

683   It is important to note that plant response to water stress is not only determined by the

684   water demand (i.e., atmospheric dryness or VPD) but also by the availability of water sources

685   (i.e., soil moisture). Although volumetric soil moisture content (θ) is often considered as a metric

686   of soil water available to plants, soil water potential (Ψ_S) is the driving force of water flows that

687   becomes available to plants by moving along gradients of water potential through the plant (stem

688   and leaf) and eventually to the air. Moreover, Ψ_S is not only determined by the θ but also by soil

689   physical properties, and thus can differ even under conditions of the same θ (Campbell, 1974;

690   van Genuchten, 1980). Unlike Ψ_S, θ is widely measured and usually available with flux data, and

691   carbon and water fluxes are often explained as a function of θ (Green et al., 2019; Novick et al.,

692   2016a). However, θ may not characterize soil moisture availability to plants properly, and its

693   relationship with carbon and water fluxes is usually nonlinear and threshold-driven (Feldman et

694   al., 2019; Novick et al., 2022; Stocker et al., 2018), making the modeling of the relationship

695   between IWUE and soil moisture availability challenging. Therefore, enhanced accessibility to

696   Ψ_S data by improving the ease and reliability of Ψ_S observations, for example, by building a

697   centralized and standardized network of Ψ (Novick et al., 2022) would be a necessary step to

698   better characterize the effect of soil moisture availability on plant responses such as IWUE and

699   mWUE.

700   In this study, we tested the two stomatal optimization models (Katul et al., 2010; Medlyn

701   et al., 2012) that are elaborations of the original Cowan & Farquhar (1977) model with few

702   modifications because our goal was to characterize variability of mWUE in response to dryness

703   (VPD and aridity index) using IWUE that can be calculated from the extensive, long-term

704   continuous data from the network of eddy covariance. Meanwhile, more recent optimization

705   models are incorporating additional physiological penalties than the water loss, for instance,

706   damage to the vascular system induced by water stress (Anderegg et al., 2018; Sperry et al.,

707   2017; Wolf et al., 2016), which may enhance prediction of long-term plant responses to climate

708   change. Although monitoring the integrity of the vascular system, which can be informed by the

709   dynamics of hydraulic conductivity, has not been widely conducted, recent advances in

710   psychrometric approaches allowing continuous measurements of plant Ψ (e.g., PSY1

711   manufactured by ICT International) and Ψ_S (e.g., TEROS 21 manufactured by Meter Group) are

712   now enabling the monitoring the dynamics of hydraulic conductivity. Moreover, the relationship

713   between plant and soil Ψ can be used to identify plant water-use strategies (e.g., isohydry

714   framework; Martinez-Vilalta et al., 2014), which can help develop m^* based on plant water-use

715   strategies. The measurements of carbon and water fluxes using the eddy covariance technique

716   with the aid of the centralized and standardized deployment of Ψ sensors (Novick et al., 2022)

37

717 will have a great potential to test models and theories of stomatal optimization and advance our

718 knowledge of it.

719

Acknowledgments

734

Author Contributions

736 K.Y., K.A.N., and D.B. conceptualized the research and developed the methodology.

737 K.Y., D.B., and M.B. analyzed the data, and K.A.N, Q.Z., L.W., T.H., X.Y., K.M., and G.B.S.

738 validated the analysis. K.Y. visualized the data analysis. K.Y. wrote the manuscript with input

739 and revisions from all authors.

740

Conflict of Interest

The authors declare that they have no conflict of interest.

743

Data Availability

The data that support the findings of this study are openly available in the FLUXNET

Data Portal at https://fluxnet.org/data/fluxnet2015-dataset/. The list of DOIs for the individual

FLUXNET sites used in this study is available in the Supporting Information (Table S1).

748

References

Allen, R. G., Pereira, L. S., Raes, D., & Smith, M. (1998). Crop evapotranspiration-Guidelines

 for computing crop water requirements-FAO Irrigation and drainage paper 56. *FAO,*

 Rome, *300*(9), D05109.

Ammann, C. (2002-2008). FLUXNET2015 CH-Oe1 Oensingen grassland [Dataset]. FLUXNET.

 https://doi.org/10.18140/FLX/1440135

Anderegg, W. R. L., Wolf, A., Arango-Velez, A., Choat, B., Chmura, D. J., Jansen, S., Kolb, T.,

 Li, S., Meinzer, F. C., Pita, P., de Dios, V. R., Sperry, J. S., Wolfe, B. T., & Pacala, S.

 (2018). Woody plants optimise stomatal behaviour relative to hydraulic risk. *Ecology*

 Letters, 21(7), 968–977. https://doi.org/10.1111/ele.12962

Anderegg, W. R. L., Wolf, A., Arango-Velez, A., Choat, B., Chmura, D. J., Jansen, S., Kolb, T.,

 Li, S., Meinzer, F., Pita, P., de Dios, V. R., Sperry, J. S., Wolfe, B. T., & Pacala, S.

 (2017). Plant water potential improves prediction of empirical stomatal models. *PLoS*

 One, *12*(10), e0185481. https://doi.org/10.1371/journal.pone.0185481

763   Ardö, J., Tahir, B., & Elkhidir, H. (2005-2009). FLUXNET2015 SD-Dem Demokeya

764   [Dataset]. FLUXNET. https://doi.org/10.18140/FLX/1440186

765   Arndt, S., Hinko-Najera, N., Griebel, A., Beringer, J., & Livesley, S. (2010-

766   2014). FLUXNET2015 AU-Wom Wombat [Dataset]. FLUXNET.

767   https://doi.org/10.18140/FLX/1440207

768   Aurela, M., Tuovinen, J. P., Hatakka, J., Lohila, A., Mäkelä, T., Rainne, J., & Lauria, T. (2001-

769   2014). FLUXNET2015 FI-Sod Sodankyla [Dataset]. FLUXNET.

770   https://doi.org/10.18140/FLX/1440160

771   Baldocchi, D. D., & Harley, P. C. (1995). Scaling carbon dioxide and water vapour exchange

772   from leaf to canopy in a deciduous forest. II. Model testing and application. *Plant, Cell &*

773   *Environment*, *18*(10), 1157–1173. https://doi.org/10.1111/j.1365-3040.1995.tb00626.x

774   Baldocchi, D., & Meyers, T. (1998). On using eco-physiological, micrometeorological and

775   biogeochemical theory to evaluate carbon dioxide, water vapor and trace gas fluxes over

776   vegetation: A perspective. *Agricultural and Forest Meteorology*, *90*(1), 1–25.

777   https://doi.org/10.1016/S0168-1923(97)00072-5

778   Baldocchi, D. D., Keeney, N., Rey-Sanchez, C., & Fisher, J. B. (2022). Atmospheric humidity

779   deficits tell us how soil moisture deficits down-regulate ecosystem evaporation. *Advances*

780   *in Water Resources*, *159*, 104100. https://doi.org/10.1016/j.advwatres.2021.104100

781   Ball, J. T., Woodrow, I. E., & Berry, J. A. (1987). A Model Predicting Stomatal Conductance

782   and its Contribution to the Control of Photosynthesis under Different Environmental

783   Conditions. In: Biggins, J. (Ed.), *Progress in Photosynthesis Research*. pp. 221–224.

784   Springer, Dordrecht. https://doi.org/10.1007/978-94-017-0519-6_48

Bassiouni, M., & Vico, G. (2021). Parsimony vs predictive and functional performance of three stomatal optimization principles in a big-leaf framework. *New Phytologist*, *231*(2), 586–600. https://doi.org/10.1111/nph.17392

Beer, C., Ciais, P., Reichstein, M., Baldocchi, D., Law, B. E., Papale, D., Soussana, J.-F., Ammann, C., Buchmann, N., Frank, D., Gianelle, D., Janssens, I. A., Knohl, A., Köstner, B., Moors, E., Roupsard, O., Verbeeck, H., Vesala, T., Williams, C. A., & Wohlfahrt, G. (2009). Temporal and among-site variability of inherent water use efficiency at the ecosystem level. *Global Biogeochemical Cycles*, *23*(2). https://doi.org/10.1029/2008GB003233

Beer, C., Reichstein, M., Tomelleri, E., Ciais, P., Jung, M., Carvalhais, N., Rodenbeck, C., Arain, M. A., Baldocchi, D., Bonan, G. B., Bondeau, A., Cescatti, A., Lasslop, G., Lindroth, A., Lomas, M., Luyssaert, S., Margolis, H., Oleson, K. W., Roupsard, O., … Papale, D. (2010). Terrestrial gross carbon dioxide uptake: Global distribution and covariation with climate. *Science*, *329*(5993), 834–838. https://doi.org/10.1126/science.1184984

Béland, M., & Baldocchi, D. D. (2021). Vertical structure heterogeneity in broadleaf forests: Effects on light interception and canopy photosynthesis. *Agricultural and Forest Meteorology*, *307*, 108525. https://doi.org/10.1016/j.agrformet.2021.108525

Béland, M., & Kobayashi, H. (2021). Mapping forest leaf area density from multiview terrestrial lidar. *Methods in Ecology and Evolution*, *12*(4), 619–633. https://doi.org/10.1111/2041-210X.13550

Belelli, L., Papale, D., & Valentini, R. (2002-2004). FLUXNET2015 RU-Ha1 Hakasia steppe [Dataset]. FLUXNET. https://doi.org/10.18140/FLX/1440184

808   Berbigier, P., Bonnefond, J., Bosc, A., Trichet, P., & Loustau, D. (1996-

809   2008). FLUXNET2015 FR-LBr Le Bray [Dataset]. FLUXNET.

810   https://doi.org/10.18140/FLX/1440163

811   Beringer, J., Cunningham, S., Baker, P., Cavagnaro, T., MacNally, R., Thompson, R., &

812   McHugh, I. (2011-2014). FLUXNET2015 AU-Whr Whroo [Dataset]. FLUXNET.

813   https://doi.org/10.18140/FLX/1440206

814   Beringer, J., & Hutley, L. (2007-2013). FLUXNET2015 AU-DaP Daly River Savanna [Dataset].

815   FLUXNET. https://doi.org/10.18140/FLX/1440123

816   Beringer, J., & Hutley, L. (2008-2014). FLUXNET2015 AU-DaS Daly River Cleared

817   [Dataset]. FLUXNET. https://doi.org/10.18140/FLX/1440122

818   Beringer, J. & Hutley, L. (2008-2014). FLUXNET2015 AU-Dry Dry River

819   [Dataset]. FLUXNET. https://doi.org/10.18140/FLX/1440197

820   Beringer, J., & Hutley, L. (2001-2014). FLUXNET2015 AU-How Howard Springs

821   [Dataset]. FLUXNET. https://doi.org/10.18140/FLX/1440125

822   Beringer, J., & Hutley, L. (2008-2014). FLUXNET2015 AU-Stp Sturt Plains

823   [Dataset]. FLUXNET. https://doi.org/10.18140/FLX/1440204

824   Beringer, J., Hutley, L., McGuire, D., Paw U, K. T., & McHugh, I. (2005-

825   2008). FLUXNET2015 AU-Wac Wallaby Creek [Dataset]. FLUXNET.

826   https://doi.org/10.18140/FLX/1440127

827   Bernhofer, C., Grünwald, T., Moderow, U., Hehn, M., Eichelmann, U., Prasse, H., & Postel,

828   U. (2004-2014). FLUXNET2015 DE-Gri Grillenburg [Dataset]. FLUXNET.

829   https://doi.org/10.18140/FLX/1440147

830   Bernhofer, C., Grünwald, T., Moderow, U., Hehn, M., Eichelmann, U., Prasse, H., & Postel,

831   U. (2008-2014). FLUXNET2015 DE-Obe Oberbärenburg [Dataset]. FLUXNET.

832   https://doi.org/10.18140/FLX/1440151

833

834   Bernhofer, C., Grünwald, T., Moderow, U., Hehn, M., Eichelmann, U., Prasse, H., & Postel,

835   U. (1996-2014). FLUXNET2015 DE-Tha Tharandt [Dataset]. FLUXNET.

836   https://doi.org/10.18140/FLX/1440152

837   Berninger, F., & Hari, P. (1993). Optimal regulation of gas exchange: Evidence from field data.

838   *Annals of Botany*, *71*(2), 135–140. https://doi.org/10.1006/anbo.1993.1017

839   Berveiller, D., Delpierre, N., Dufrêne, E., Pontailler, J. Y., Vanbostal, L., Janvier, B., Mottet, L.,

840   & Cristinacce, K. (2005-2014). FLUXNET2015 FR-Fon Fontainebleau-Barbeau

841   [Dataset]. FLUXNET. https://doi.org/10.18140/FLX/1440161

842   Bonal, D., & Burban, B. (2004-2014). FLUXNET2015 GF-Guy Guyaflux (French Guiana)

843   [Dataset]. FLUXNET. https://doi.org/10.18140/FLX/1440165

844   Bonan, G. B., Williams, M., Fisher, R. A., & Oleson, K. W. (2014). Modeling stomatal

845   conductance in the earth system: Linking leaf water-use efficiency and water transport

846   along the soil-plant-atmosphere continuum. *Geoscientific Model Development*, *7*(5),

847   2193–2222. https://doi.org/10.5194/gmd-7-2193-2014

848   Brodribb, T. J., Holbrook, N. M., Zwieniecki, M. A., & Palma, B. (2005). Leaf hydraulic

849   capacity in ferns, conifers and angiosperms: Impacts on photosynthetic maxima. *New*

850   *Phytologist*, *165*(3), 839–846. https://doi.org/10.1111/j.1469-8137.2004.01259.x

851   Brümmer, C., Lucas-Moffat, A., Herbst, M., Kolle, O., & Delorme, J. P. (2001-

852   2014). FLUXNET2015 DE-Geb Gebesee [Dataset]. FLUXNET.

853   https://doi.org/10.18140/FLX/1440146

854   Buckley, T. N. (2017). Modeling stomatal conductance. *Plant Physiology*, *174*(2), 572–582.

855   https://doi.org/10.1104/pp.16.01772

856   Buysse, P., Durand, B., Gueudet, J. C., Mascher, N., Larmanou, E., Cellier, P., & Loubet,

857   B. (2004-2014). FLUXNET2015 FR-Gri Grignon [Dataset]. FLUXNET.

858   https://doi.org/10.18140/FLX/1440162

859   Von Caemmerer, S. (2000). *Biochemical models of leaf photosynthesis*. Csiro publishing.

860   https://doi.org/10.1071/9780643103405

861   Campbell, G. S. (1974). A simple method for determining unsaturated conductivity from

862   moisture retention data. *Soil Science*, *117*(6), 311-314. https://doi.org/10.1097/00010694-

863   197406000-00001

864   Cañete, E., Ortiz, P., Jiménez, M., Poveda, F., Priego, O., Ballesteros, A., & Kowalski, A. (2004-

865   2013). FLUXNET2015 ES-LJu Llano de los Juanes [Dataset]. FLUXNET.

866   https://doi.org/10.18140/FLX/1440157

867   Cleverly, J., Eamus, D., & Isaac, P. (2010-2014). FLUXNET2015 AU-ASM Alice Springs

868   [Dataset]. FLUXNET. https://doi.org/10.18140/FLX/1440194

869   Cleverly, J., Eamus, D., Isaac, P. (2012-2014). FLUXNET2015 AU-TTE Ti Tree East [Dataset].

870   FLUXNET. https://doi.org/10.18140/FLX/1440205

871   Cowan, I. R. (1982). Regulation of Water Use in Relation to Carbon Gain in Higher Plants. In:

872   O. L. Lange, P. S. Nobel, C. B. Osmond, & H. Ziegler (Eds.), *Physiological Plant*

Ecology II: Water Relations and Carbon Assimilation, pp. 589–613. Springer. https://doi.org/10.1007/978-3-642-68150-9_18

Cowan, I. R., & Farquhar, G. D. (1977). Stomatal function in relation to leaf metabolism and environment. *Symposia of the Society for Experimental Biology*, *31*, 471–505.

Cremonese, E., Galvagno, M., di Cella, U., & Migliavacca, M. (2008-2014). FLUXNET2015 IT-Tor Torgnon [Dataset]. FLUXNET. https://doi.org/10.18140/FLX/1440237

Dolman, H., van der Molen, M., Parmentier, F. J., Marchesini, L., Dean, J., van Huissteden, K., & Maximov, T. (2003-2014). FLUXNET2015 RU-Cok Chokurdakh [Dataset]. FLUXNET. https://doi.org/10.18140/FLX/1440182

Dong, G. (2007-2010). FLUXNET2015 CN-Cng Changling [Dataset]. FLUXNET. https://doi.org/10.18140/FLX/1440209

Farquhar, G. D. (1978). Feedforward responses of stomata to humidity. *Australian Journal of Plant Physiology, 5*(6), 787–800. https://doi.org/10.1071/PP9780787

Farquhar, G. D., von Caemmerer, S., & Berry, J. A. (1980a). A biochemical model of photosynthetic CO_2 assimilation in leaves of C_3 species. *Planta*, *149*(1), 78–90. https://doi.org/10.1007/BF00386231

Farquhar, G. D., Schulze, E. D., & Kuppers, M. (1980b). Responses to humidity by stomata of *Nicotiana glauca* L. and *Corylus avellana* L. are consistent with the optimization of carbon dioxide uptake with respect to water loss. *Australian Journal of Plant Physiology*, *7*(3), 315–327. https://doi.org/10.1071/PP9800315

Feldman, A. F., Short Gianotti, D. J., Trigo, I. F., Salvucci, G. D., & Entekhabi, D. (2019). Satellite-based assessment of land surface energy partitioning–soil moisture relationships

and effects of confounding variables. *Water Resources Research*, *55*(12), 10657–10677.

https://doi.org/10.1029/2019WR025874

Feng, X., Lu, Y., Jiang, M., Katul, G., Manzoni, S., Mrad, A., & Vico, G. (2022). Instantaneous

stomatal optimization results in suboptimal carbon gain due to legacy effects. *Plant, Cell*

& Environment, 45(11), 3189–3204. https://doi.org/10.1111/pce.14427

Ficklin, D. L., & Novick, K. A. (2017). Historic and projected changes in vapor pressure deficit

suggest a continental-scale drying of the United States atmosphere. *Journal of*

Geophysical Research: Atmospheres, *122*(4), 2061–2079.

https://doi.org/10.1002/2016JD025855

Finnigan, J. J., & Raupach, M. R. (1987). Transfer processes in plant canopies in relation to

stomatal characteristics. *Stomatal Function*, 385–429.

https://www.cabdirect.org/cabdirect/abstract/19880712530

Fites, J. A., & Teskey, R. O. (1988). CO_2 and water vapor exchange of *Pinustaeda* in relation to

stomatal behavior: Test of an optimization hypothesis. *Canadian Journal of Forest*

Research, *18*(2), 150–157. https://doi.org/10.1139/x88-024

FLUXNET2015 CA-NS1 UCI-1850 burn site [Dataset]. (2001-2005).

FLUXNET. https://doi.org/10.18140/FLX/1440036

FLUXNET2015 CA-NS2 UCI-1930 burn site [Dataset]. (2001-2005).

FLUXNET. https://doi.org/10.18140/FLX/1440037

FLUXNET2015 CA-NS3 UCI-1964 burn site [Dataset]. (2001-2005). FLUXNET.

https://doi.org/10.18140/FLX/1440038

FLUXNET2015 CA-NS4 UCI-1964 burn site wet [Dataset]. (2002-2005). FLUXNET.

https://doi.org/10.18140/FLX/1440039

918   FLUXNET2015 CA-NS5 UCI-1981 burn site [Dataset]. (2001-2005). FLUXNET.

919   https://doi.org/10.18140/FLX/1440040

920   FLUXNET2015 CA-NS6 UCI-1989 burn site [Dataset]. (2001-2005). FLUXNET.

921   https://doi.org/10.18140/FLX/1440041

922   FLUXNET2015 CA-NS7 UCI-1998 burn site [Dataset]. (2002-2005). FLUXNET.

923   https://doi.org/10.18140/FLX/1440042

924   FLUXNET2015 CA-Oas Saskatchewan - Western Boreal, Mature Aspen [Dataset]. (1996-2010).

925   FLUXNET. https://doi.org/10.18140/FLX/1440043

926   FLUXNET2015 CA-Obs Saskatchewan - Western Boreal, Mature Black Spruce [Dataset].

927   (1997-2010). FLUXNET. https://doi.org/10.18140/FLX/1440044

928   FLUXNET2015 CA-Qfo Quebec - Eastern Boreal, Mature Black Spruce [Dataset]. (2003-2010).

929   FLUXNET. https://doi.org/10.18140/FLX/1440045

930   FLUXNET2015 CA-SF1 Saskatchewan - Western Boreal, forest burned in 1977 [Dataset].

931   (2003-2006). FLUXNET. https://doi.org/10.18140/FLX/1440046

932   FLUXNET2015 CA-SF2 Saskatchewan - Western Boreal, forest burned in 1989 [Dataset].

933   (2001-2005). FLUXNET. https://doi.org/10.18140/FLX/1440047

934   FLUXNET2015 CA-SF3 Saskatchewan - Western Boreal, forest burned in 1998 [Dataset].

935   (2001-2006). FLUXNET. https://doi.org/10.18140/FLX/1440048

936   FLUXNET2015 CA-TP1 Ontario - Turkey Point 2002 Plantation White Pine [Dataset]. (2002-

937   2014). FLUXNET. https://doi.org/10.18140/FLX/1440050

938   FLUXNET2015 CA-TP2 Ontario - Turkey Point 1989 Plantation White Pine [Dataset]. (2002-

939   2007). FLUXNET. https://doi.org/10.18140/FLX/1440051

940   FLUXNET2015 CA-TP3 Ontario - Turkey Point 1974 Plantation White Pine [Dataset]. (2002-

941   2014). FLUXNET. https://doi.org/10.18140/FLX/1440052

942   FLUXNET2015 CA-TP4 Ontario - Turkey Point 1939 Plantation White Pine [Dataset]. (2002-

943   2014). FLUXNET. https://doi.org/10.18140/FLX/1440053

944   FLUXNET2015 CA-TPD Ontario - Turkey Point Mature Deciduous [Dataset]. (2012-

945   2014). FLUXNET. https://doi.org/10.18140/FLX/1440112

946   FLUXNET2015 US-AR1 ARM USDA UNL OSU Woodward Switchgrass 1 [Dataset]. (2009-

947   2012). FLUXNET. https://doi.org/10.18140/FLX/1440103

948   FLUXNET2015 US-AR2 ARM USDA UNL OSU Woodward Switchgrass 2 [Dataset]. (2009-

949   2012). FLUXNET. https://doi.org/10.18140/FLX/1440104

950   FLUXNET2015 US-ARM ARM Southern Great Plains site- Lamont [Dataset]. (2003-2012).

951   FLUXNET. https://doi.org/10.18140/FLX/1440066

952   FLUXNET2015 US-Blo Blodgett Forest [Dataset]. (1997-2007).

953   FLUXNET. https://doi.org/10.18140/FLX/1440068

954   FLUXNET2015 US-CRT Curtice Walter-Berger cropland [Dataset]. (2011-2013). FLUXNET.

955   https://doi.org/10.18140/FLX/1440117

956   FLUXNET2015 US-Cop Corral Pocket [Dataset]. (2001-2007).

957   FLUXNET. https://doi.org/10.18140/FLX/1440100

958   FLUXNET2015 US-GLE GLEES [Dataset]. (2004-2014).

959   FLUXNET. https://doi.org/10.18140/FLX/1440069

960   FLUXNET2015 US-Ha1 Harvard Forest EMS Tower (HFR1) [Dataset]. (1991-2012).

961   FLUXNET. https://doi.org/10.18140/FLX/1440071

962   FLUXNET2015 US-IB2 Fermi National Accelerator Laboratory- Batavia (Prairie site)

963   [Dataset]. (2004-2011). FLUXNET. https://doi.org/10.18140/FLX/1440072

964   FLUXNET2015 US-KS2 Kennedy Space Center (scrub oak) [Dataset]. (2003-2006).

965   FLUXNET. https://doi.org/10.18140/FLX/1440075

966   FLUXNET2015 US-Me2 Metolius mature ponderosa pine [Dataset]. (2002-2014). FLUXNET.

967   https://doi.org/10.18140/FLX/1440079

968   FLUXNET2015 US-Me3 Metolius-second young aged pine [Dataset]. (2004-2009).

969   FLUXNET. https://doi.org/10.18140/FLX/1440080

970   FLUXNET2015 US-Me4 Metolius-old aged ponderosa pine [Dataset]. (1996-2000).

971   FLUXNET. https://doi.org/10.18140/FLX/1440081

972   FLUXNET2015 US-Me5 Metolius-first young aged pine [Dataset]. (2000-

973   2002). FLUXNET. https://doi.org/10.18140/FLX/1440082

974   FLUXNET2015 US-Me6 Metolius Young Pine Burn [Dataset]. (2010-2014).

975   FLUXNET. https://doi.org/10.18140/FLX/1440099

976   FLUXNET2015 US-MMS Morgan Monroe State Forest [Dataset]. (1999-2014).

977   FLUXNET. https://doi.org/10.18140/FLX/1440083

978   FLUXNET2015 US-Ne3 Mead - rainfed maize-soybean rotation site [Dataset]. (2001-2013).

979   FLUXNET. https://doi.org/10.18140/FLX/1440086

980   FLUXNET2015 US-NR1 Niwot Ridge Forest (LTER NWT1) [Dataset]. (1998-2014).

981   FLUXNET. https://doi.org/10.18140/FLX/1440087

982   FLUXNET2015 US-Oho Oak Openings [Dataset]. (2004-2013).

983   FLUXNET. https://doi.org/10.18140/FLX/1440088

984   FLUXNET2015 US-SRC Santa Rita Creosote [Dataset]. (2008-2014).

985   FLUXNET. https://doi.org/10.18140/FLX/1440098

986   FLUXNET2015 US-SRG Santa Rita Grassland [Dataset]. (2008-2014).

987   FLUXNET. https://doi.org/10.18140/FLX/1440114

988   FLUXNET2015 US-SRM Santa Rita Mesquite [Dataset]. (2004-2014).

989   FLUXNET. https://doi.org/10.18140/FLX/1440090

990   FLUXNET2015 US-Ton Tonzi Ranch [Dataset]. (2001-2014) .

991   FLUXNET. https://doi.org/10.18140/FLX/1440092

992   FLUXNET2015 US-Twt Twitchell Island [Dataset]. (2009-2014).

993   FLUXNET. https://doi.org/10.18140/FLX/1440106

994   FLUXNET2015 US-UMB Univ. of Mich. Biological Station [Dataset]. (2000-2014).

995   FLUXNET. https://doi.org/10.18140/FLX/1440093

996   FLUXNET2015 US-Var Vaira Ranch- Ione [Dataset]. (2000-2014).

997   FLUXNET. https://doi.org/10.18140/FLX/1440094

998   FLUXNET2015 US-Whs Walnut Gulch Lucky Hills Shrub [Dataset]. (2007-2014).

999   FLUXNET. https://doi.org/10.18140/FLX/1440097

1000   FLUXNET2015 US-Wi4 Mature red pine (MRP) [Dataset]. (2002-2005).

1001   FLUXNET. https://doi.org/10.18140/FLX/1440058

1002   FLUXNET2015 US-Wkg Walnut Gulch Kendall Grasslands [Dataset]. (2004-2014).

1003   FLUXNET. https://doi.org/10.18140/FLX/1440096

1004   Franks, P. J., Bonan, G. B., Berry, J. A., Lombardozzi, D. L., Holbrook, N. M., Herold, N., &

1005   Oleson, K. W. (2018). Comparing optimal and empirical stomatal conductance models

for application in Earth system models. *Global Change Biology*, *24*(12), 5708–5723. https://doi.org/10.1111/gcb.14445

van Genuchten, M. Th. (1980). A closed-form equation for predicting the hydraulic conductivity of unsaturated soils. *Soil Science Society of America Journal*, *44*(5), 892–898. https://doi.org/10.2136/sssaj1980.03615995004400050002x

Gianelle, D., Cavagna, M., Zampedri, R., & Marcolla, B. (2003-2013). FLUXNET2015 IT-MBo Monte Bondone [Dataset]. FLUXNET. https://doi.org/10.18140/FLX/1440170

Gianelle, D., Zampedri, R., Cavagna, M., & Sottocornola, M. (2003-2014). FLUXNET2015 IT-Lav Lavarone [Dataset]. FLUXNET. https://doi.org/10.18140/FLX/1440169

Green, J. K., Seneviratne, S. I., Berg, A. M., Findell, K. L., Hagemann, S., Lawrence, D. M., & Gentine, P. (2019). Large influence of soil moisture on long-term terrestrial carbon uptake. *Nature*, *565*(7740), 476–479. https://doi.org/10.1038/s41586-018-0848-x

Grieu, P., Guehl, J. M., & Aussenac, G. (1988). The effects of soil and atmospheric drought on photosynthesis and stomatal control of gas exchange in three coniferous species. *Physiologia Plantarum*, *73*(1), 97–104. https://doi.org/10.1111/j.1399-3054.1988.tb09199.x

Grossiord, C., Buckley, T. N., Cernusak, L. A., Novick, K. A., Poulter, B., Siegwolf, R. T. W., Sperry, J. S., & McDowell, N. G. (2020). Plant responses to rising vapor pressure deficit. *New Phytologist*, *226*(6), 1550–1566. https://doi.org/10.1111/nph.16485

Gruening, C., Goded, I., Cescatti, A., Manca, G., & Seufert, G. (1999-2012). FLUXNET2015 IT-SRo San Rossore [Dataset]. FLUXNET. https://doi.org/10.18140/FLX/1440176

Hall, A. E., & Schulze, E.-D. (1980). Stomatal response to environment and a possible

    interrelation between stomatal effects on transpiration and CO_2 assimilation. *Plant, Cell*

    & Environment, *3*(6), 467–474. https://doi.org/10.1111/1365-3040.ep11587040

Hari, P., Mäkelä, A., & Pohja, T. (2000). Surprising implications of the optimality hypothesis of

    stomatal regulation gain support in a field test. *Functional Plant Biology*, *27*(1), 77–80.

    https://doi.org/10.1071/pp99050

Hörtnagl, L., Eugster, W., Merbold, L., Buchmann, N., Gharun, M., Etzold, S., Haesler, R.,

    Haeni, M., Pluess, P., Meier, P., Käslin, F., & Baur, T. (1997-

    2014). FLUXNET2015 CH-Dav Davos [Dataset].

    FLUXNET. https://doi.org/10.18140/FLX/1440132

Hörtnagl, L., Feigenwinter, I., Fuchs, K., Merbold, L., Buchmann, N.,

    Eugster, W., Zeeman, M., Baur, T., Pluess, P., Käslin, F., Meier, P., & Koller, P. (2005-

    2014). FLUXNET2015 CH-Cha Chamau [Dataset]. FLUXNET.

    https://doi.org/10.18140/FLX/1440131

Hörtnagl, L., Feigenwinter, I., Fuchs, K., Merbold, L., Buchmann, N., Eugster, W., Zeeman, M.,

    Baur, T., Pluess, P., Käslin, F., Meier, P., & Koller, P. (2005-2014). FLUXNET2015 CH-

    Fru Früebüel [Dataset]. FLUXNET. https://doi.org/10.18140/FLX/1440133

Ibrom, A., & Pilegaard, K. (1996-2014). FLUXNET2015 DK-Sor Soroe [Dataset]. FLUXNET.

    https://doi.org/10.18140/FLX/1440155

Jones, H. G. (2014). Plants and Microclimate: A Quantitative Approach to Environmental Plant

    Physiology. 3rd ed. Cambridge University Press.

Katul, G. G., Palmroth, S., & Oren, R. (2009). Leaf stomatal responses to vapour pressure deficit

    under current and CO_2-enriched atmosphere explained by the economics of gas exchange.

Plant, Cell & Environment, *32*(8), 968–979. https://doi.org/10.1111/j.1365-3040.2009.01977.x

Katul, G., Manzoni, S., Palmroth, S., & Oren, R. (2010). A stomatal optimization theory to describe the effects of atmospheric CO_2 on leaf photosynthesis and transpiration. *Annals of Botany*, *105*(3), 431–442. https://doi.org/10.1093/aob/mcp292

Kelliher, F. M., Leuning, R., Raupach, M. R., & Schulze, E.-D. (1995). Maximum conductances for evaporation from global vegetation types. *Agricultural and Forest Meteorology*, *73*(1), 1–16. https://doi.org/10.1016/0168-1923(94)02178-M

Kennedy, D., Swenson, S., Oleson, K. W., Lawrence, D M., Fisher, R., Lola da Costa, A. C., & Gentine, P. (2019). Implementing plant hydraulics in the Community Land Model, version 5. *Journal of Advances in Modeling Earth Sysntems, 11*(2), 485–513. https://doi.org/10.1029/2018MS001500

Knauer, J., Werner, C., & Zaehle, S. (2015). Evaluating stomatal models and their atmospheric drought response in a land surface scheme: A multibiome analysis. *Journal of Geophysical Research: Biogeosciences*, *120*(10), 1894–1911. https://doi.org/10.1002/2015JG003114

Knauer, J., Zaehle, S., Medlyn, B. E., Reichstein, M., Williams, C. A., Migliavacca, M., De Kauwe, M. G., Werner, C., Keitel, C., Kolari, P., Limousin, J.-M., & Linderson, M.-L. (2018). Towards physiologically meaningful water-use efficiency estimates from eddy covariance data. *Global Change Biology*, *24*(2), 694–710. https://doi.org/10.1111/gcb.13893

Knohl, A., Tiedemann, F., Kolle, O., Schulze, E. D., Anthoni, P., Kutsch, W., Herbst, M., &

 Siebicke, L. (2002-2012). FLUXNET2015 DE-Lnf Leinefelde [Dataset]. FLUXNET.

 https://doi.org/10.18140/FLX/1440150

Knohl, A., Tiedemann, F., Kolle, O., Schulze, E. D., Kutsch, W., Herbst, M., & Siebicke,

 L. (2000-2012). FLUXNET2015 DE-Hai Hainich [Dataset]. FLUXNET.

 https://doi.org/10.18140/FLX/1440148

Kutsch, W., Merbold, L., & Kolle, O. (2000-2009). FLUXNET2015 ZM-Mon Mongu [Dataset].

 FLUXNET. https://doi.org/10.18140/FLX/1440189

Lanning, M., Wang, L., & Novick, K. A. (2020). The importance of cuticular permeance in

 assessing plant water–use strategies. *Tree Physiology*, *40*(4), 425–432.

 https://doi.org/10.1093/treephys/tpaa020

Lasslop, G., Reichstein, M., Papale, D., Richardson, A. D., Arneth, A., Barr, A., Stoy, P., &

 Wohlfahrt, G. (2010). Separation of net ecosystem exchange into assimilation and

 respiration using a light response curve approach: critical issues and global evaluation.

 Global Change Biology, 16(1), 187–208. https://doi.org/10.1111/j.1365-

 2486.2009.02041.x

Lawlor, D. W., & Tezara, W. (2009). Causes of decreased photosynthetic rate and metabolic

 capacity in water-deficient leaf cells: A critical evaluation of mechanisms and integration

 of processes. *Annals of Botany*, *103*(4), 561–579. https://doi.org/10.1093/aob/mcn244

Leuning, R. (1995). A critical appraisal of a combined stomatal-photosynthesis model for C_3

 plants. *Plant, Cell & Environment.*, *18*(4), 339–355. https://doi.org/10.1111/j.1365-

 3040.1995.tb00370.x

1094   Lin, C., Gentine, P., Huang, Y., Guan, K., Kimm, H., & Zhou, S. (2018). Diel ecosystem

1095   conductance response to vapor pressure deficit is suboptimal and independent of soil

1096   moisture. *Agricultural and Forest Meteorology*, *250–251*, 24–34.

1097   https://doi.org/10.1016/j.agrformet.2017.12.078

1098   Lin, Y.-S., Medlyn, B. E., Duursma, R. A., Prentice, I. C., Wang, H., Baig, S., Eamus, D., de

1099   Dios, V. R., Mitchell, P., Ellsworth, D. S., de Beeck, M. O., Wallin, G., Uddling, J.,

1100   Tarvainen, L., Linderson, M.-L., Cernusak, L. A., Nippert, J. B., Ocheltree, T. W.,

1101   Tissue, D. T., … Wingate, L. (2015). Optimal stomatal behaviour around the world.

1102   *Nature Climate Change*, *5*(5), 459–464. https://doi.org/10.1038/nclimate2550

1103   Lindauer, M., Steinbrecher, R., Wolpert, B., Mauder, M., & Schmid, H. (2009-

1104   2013). FLUXNET2015 DE-Lkb Lackenberg [Dataset]. FLUXNET.

1105   https://doi.org/10.18140/FLX/1440214

1106   Lohila, A., Aurela, M., Tuovinen, J. P., Hatakka, J., & Laurila, T. (2000-

1107   2003). FLUXNET2015 FI-Jok Jokioinen [Dataset]. FLUXNET.

1108   https://doi.org/10.18140/FLX/1440159

1109   Lohila, A., Korkiakoski, M., Tuovinen, J. P., Hatakka, J., Aurela, M., Rainne, J., Mäkelä, T., &

1110   Laurila, T. (2009-2012). FLUXNET2015 FI-Let Lettosuo [Dataset]. FLUXNET.

1111   https://doi.org/10.18140/FLX/1440227

1112   Loveland, T. R., & Belward, A. S. (1997). The International Geosphere Biosphere Programme

1113   Data and Information System global land cover data set (DISCover). *Acta Astronautica*,

1114   *41*(4-10), 681–689. https://doi.org/10.1016/S0094-5765(98)00050-2

Lu, Y., Duursma, R. A., Farrior, C. E., Medlyn, B. E., & Feng, X. (2020). Optimal stomatal

drought response shaped by competition for water and hydraulic risk can explain plant

trait covariation. *New Phytologist*, *225*(3), 1206–1217. https://doi.org/10.1111/nph.16207

Lu, Y. J., Duursma, R. A., & Medlyn, B. E. (2016). Optimal stomatal behaviour under stochastic

rainfall. *Journal of Theoretical Biology*, *394*, 160–171.

https://doi.org/10.1016/j.jtbi.2016.01.003

Lund, M., Jackowicz-Korczyński, M., & Abermann, J. (2000-2014). FLUXNET2015 GL-

ZaH Zackenberg Heath [Dataset]. FLUXNET. https://doi.org/10.18140/FLX/1440224

Macfarlane, C., Lambert, P., Byrne, J., Johnstone, C., & Smart, N. (2011-

2014). FLUXNET2015 AU-Gin Gingin [Dataset].

FLUXNET. https://doi.org/10.18140/FLX/1440199

Magliulo, V., Tommasi, P., Famulari, D., Gasbarra, D., Vitale, L., Manco, A., Esposito, A.,

Tosca, M., & di Matteo, F. (2004-2014). FLUXNET2015 IT-BCi Borgo Cioffi

[Dataset]. FLUXNET. https://doi.org/10.18140/FLX/1440166

Mäkelä, A., Berninger, F., & Hari, P. (1996). Optimal control of gas exchange during drought:

Theoretical analysis. *Annals of Botany*, *77*(5), 461–467.

https://www.jstor.org/stable/42764687

Mammarella, I., Keronen, P., Kolari, P., Launiainen, S., Pumpanen, J., Rannik, Ü., Siivola,

E., Levula, J., Pohja, T., & Vesala, T. (1996-2014). FLUXNET2015 FI-Hyy Hyytiala

[Dataset]. FLUXNET. https://doi.org/10.18140/FLX/1440158

Manca, G., & Goded, I. (2002-2004). FLUXNET2015 IT-PT1 Parco Ticino forest [Dataset].

FLUXNET. https://doi.org/10.18140/FLX/1440172

Manzoni, S., Vico, G., Katul, G., Fay, P. A., Polley, W., Palmroth, S., & Porporato, A. (2011).
Optimizing stomatal conductance for maximum carbon gain under water stress: A meta-
analysis across plant functional types and climates. *Functional Ecology*, *25*(3), 456–467.
https://doi.org/10.1111/j.1365-2435.2010.01822.x

Manzoni, S., Vico, G., Palmroth, S., Porporato, A., & Katul, G. (2013). Optimization of stomatal
conductance for maximum carbon gain under dynamic soil moisture. *Advances in Water
Resources*, *62*, 90–105. https://doi.org/10.1016/j.advwatres.2013.09.020

Marshall, B. & Biscoe, P. V. (1980). A model for C_3 leaves describing the dependence of net
photosynthesis on irradiance, *Journal of Experimental Botany, 31*(1), 29–
39. https://doi.org/10.1093/jxb/31.1.29

Martinez-Vilalta, J., Poyatos, R., Aguade, D., Retana, J., & Mencuccini, M. (2014). A new look
at water transport regulation in plants. *New Phytologist*, *204*(1), 105–115.
https://doi.org/10.1111/nph.12912

Matteucci, G. (1996-2014). FLUXNET2015 IT-Col Collelongo [Dataset].
FLUXNET. https://doi.org/10.18140/FLX/1440167

Medlyn, B. E., De Kauwe, M. G., Lin, Y.-S., Knauer, J., Duursma, R. A., Williams, C. A.,
Arneth, A., Clement, R., Isaac, P., Limousin, J.-M., Linderson, M.-L., Meir, P., Martin-
StPaul, N., & Wingate, L. (2017). How do leaf and ecosystem measures of water-use
efficiency compare? *New Phytologist, 216*(3), 758–770.
https://doi.org/10.1111/nph.14626.

Medlyn, B. E., Duursma, R. A., Eamus, D., Ellsworth, D. S., Colin Prentice, I., Barton, C. V. M.,
Crous, K. Y., de Angelis, P., Freeman, M., & Wingate, L. (2012). Reconciling the

optimal and empirical approaches to modelling stomatal conductance. *Global Change Biology*, *18*(11), 3476–3476. https://doi.org/10.1111/j.1365-2486.2012.02790.x

Meyer, W., Cale, P., Koerber, G., Ewenz, C., & Sun, Q. (2010-2014). FLUXNET2015 AU-Cpr Calperum [Dataset]. FLUXNET. https://doi.org/10.18140/FLX/1440195

Michaelis, L. & Menten, M. L. (1913). Die kinetik der invertinwirkung. *Biochem. z*, *49*(333-369), 352.

Montagnani, L., & Minerbi, S. (1998-2013). FLUXNET2015 IT-Ren Renon [Dataset]. FLUXNET. https://doi.org/10.18140/FLX/1440173

Monteith, J. L. (1965). Evaporation and environment. *Symposia of the Society for Experimental Biology,* 19, 205–234.

Moors, E., & Elbers, J. (1996-2014). FLUXNET2015 NL-Loo Loobos [Dataset]. FLUXNET. https://doi.org/10.18140/FLX/1440178

Nouvellon, Y. (2006-2009). FLUXNET2015 CG-Tch Tchizalamou [Dataset]. FLUXNET. https://doi.org/10.18140/FLX/1440142

Novick, K. A., & Barnes, M. L. (2023). A practical exploration of land cover impacts on surface and air temperature when they are most consequential. *Environmental Research: Climate, 2*(2), 025007. https://doi.org/10.1088/2752-5295/accdf9

Novick, K. A., Ficklin, D. L., Baldocchi, D., Davis, K. J., Ghezzehei, T. A., Konings, A. G., MacBean, N., Raoult, N., Scott, R. L., Shi, Y., Sulman, B. N., & Wood, J. D. (2022). Confronting the water potential information gap. *Nature Geoscience*, *15*, 158–164. https://doi.org/10.1038/s41561-022-00909-2

Novick, K. A., Ficklin, D. L., Stoy, P. C., Williams, C. A., Bohrer, G., Oishi, A. C., Papuga, S. A., Blanken, P. D., Noormets, A., Sulman, B. N., Scott, R. L., Wang, L., & Phillips, R. P.

(2016a). The increasing importance of atmospheric demand for ecosystem water and carbon fluxes. *Nature Climate Change, 6*, 1023–1027. https://doi.org/10.1038/nclimate3114

Novick, K. A., Konings, A. G., & Gentine, P. (2019). Beyond soil water potential: An expanded view on isohydricity including land-atmosphere interactions and phenology. *Plant, Cell & Environment*, 42(6), 1802–1815. https://doi.org/10.1111/pce.13517

Novick, K. A., Miniat, C. F., & Vose, J. M. (2016b). Drought limitations to leaf-level gas exchange: Results from a model linking stomatal optimization and cohesion-tension theory. *Plant, Cell & Environment*, *39*(3), 583–596. https://doi.org/10.1111/pce.12657

Ourcival, J. M., Piquemal, K., Joffre, R., & Jean-Marc, L. (2000-2014). FLUXNET2015 FR-Pue Puechabon [Dataset]. FLUXNET. https://doi.org/10.18140/FLX/1440164

Papale, D., Arriga, N., Belelli, L., Consalvo, C., Dore, S., Manca, G., Mazzenga, F., Sabbatini, S., Stefani, P., Tirone, G., Valentini, R., Boschi, A., & Tomassucci, M. (2002-2012). FLUXNET2015 IT-Ro2 Roccarespampani 2 [Dataset]. FLUXNET. https://doi.org/10.18140/FLX/1440175

Pastorello, G., Trotta, C., Canfora, E., Chu, H., Christianson, D., Cheah, Y.-W., Poindexter, C., Chen, J., Elbashandy, A., Humphrey, M., Isaac, P., Polidori, D., Reichstein, M., Ribeca, A., van Ingen, C., Vuichard, N., Zhang, L., Amiro, B., Ammann, C., … Papale, D. (2020). The FLUXNET2015 dataset and the ONEFlux processing pipeline for eddy covariance data. *Scientific Data*, *7*, 225. https://doi.org/10.1038/s41597-020-0534-3

Paw U, K. T., & Meyers, T. P. (1989). Investigations with a higher-order canopy turbulence model into mean source-sink levels and bulk canopy resistances. *Agricultural and Forest Meteorology*, *47*(2), 259–271. https://doi.org/10.1016/0168-1923(89)90099-3

Pendall, E., Griebel, A., Metzen, D., & Barton, C. (2012-2014). FLUXNET2015 AU-

Cum Cumberland Plain [Dataset]. FLUXNET. https://doi.org/10.18140/FLX/1440196

Pilegaard, K., & Ibrom, A. (2005-2008). FLUXNET2015 DK-Eng Enghave

[Dataset]. FLUXNET. https://doi.org/10.18140/FLX/1440153

Posse, G., Lewczuk, N., Richter, K., & Cristiano, P. (2009-2012). FLUXNET2015 AR-Vir

Virasoro [Dataset]. FLUXNET. https://doi.org/10.18140/FLX/1440192

Poveda, F., Ballesteros, A., Cañete, E., Ortiz, P., Jiménez, M., Priego, O., & Kowalski, A. (2007-

2012). FLUXNET2015 ES-Amo Amoladeras [Dataset]. FLUXNET.

https://doi.org/10.18140/FLX/1440156

Reverter, B., Perez-Cañete, E., & Kowalski, A. (2007-2009). FLUXNET2015 ES-LgS Laguna

Seca [Dataset]. FLUXNET. https://doi.org/10.18140/FLX/1440225

Sabbatini, S., Arriga, N., Matteucci, G., Papale, D., Tomassucci, M., & Boschi, A. (2011-

2014). FLUXNET2015 IT-CA3 Castel d'Asso3 [Dataset]. FLUXNET.

https://doi.org/10.18140/FLX/1440232

Sabbatini, S., Arriga, N., Papale, D., Tomassucci, M., & Boschi, A. (2011-

2014). FLUXNET2015 IT-CA1 Castel d'Asso1 [Dataset]. FLUXNET.

https://doi.org/10.18140/FLX/1440230

Sabot, M. E. B., De Kauwe, M. G., Pitman, A. J., Medlyn, B. E., Ellsworth, D. S., Martin-StPaul,

N. K., Wu, J., Choat, B., Limousin, J.-M., Mitchell, P. J., Rogers, A., & Serbin, S. P.

(2022). One stomatal model to rule them all? Toward improved representation of carbon

and water exchange in global models. *Journal of Advances in Modeling Earth Systems*,

14(4), e2021MS002761. https://doi.org/10.1029/2021MS002761

Schneider, K., & Schmidt, M. (2007-2010). FLUXNET2015 DE-Seh Selhausen

[Dataset]. FLUXNET. https://doi.org/10.18140/FLX/1440217

Schroder, I., Zegelin, S., Palu, T., & Feitz, A. (2011-2013). FLUXNET2015 AU-Emr Emerald

[Dataset]. FLUXNET. https://doi.org/10.18140/FLX/1440198

Sigut, L., Havrankova, K., Jocher, G., Pavelka, M., Janouš, D., Stanik, K., Trusina, J., & Czerny,

R. (2004-2014). FLUXNET2015 CZ-BK1 Bily Kriz forest [Dataset].

FLUXNET. https://doi.org/10.18140/FLX/1440143

Sigut, L., Havrankova, K., Jocher, G., Pavelka, M., Janouš, D., Stanik, K., Trusina, J., & Czerny,

R. (2004-2012). FLUXNET2015 CZ-BK2 Bily Kriz grassland [Dataset]. FLUXNET.

https://doi.org/10.18140/FLX/1440144

Spano, D., Duce, P., Marras, S., Sirca, C., Mereu, S., Arca, A., Zara, P., Ventura, A., & Sanna,

L. (2004-2014). FLUXNET2015 IT-Noe Arca di Noe - Le Prigionette

[Dataset]. FLUXNET. https://doi.org/10.18140/FLX/1440171

Sperry, J. S., Venturas, M. D., Anderegg, W. R. L., Mencuccini, M., Mackay, D. S., Wang, Y., &

Love, D. M. (2017). Predicting stomatal responses to the environment from the

optimization of photosynthetic gain and hydraulic cost. *Plant, Cell & Environment*,

40(6), 816–830. https://doi.org/10.1111/pce.12852

Stocker, B. D., Zscheischler, J., Keenan, T. F., Prentice, I. C., Peñuelas, J., & Seneviratne, S. I.

(2018). Quantifying soil moisture impacts on light use efficiency across biomes. *New

Phytologist*, *218*(4), 1430–1449. https://doi.org/10.1111/nph.15123

Thornley, J. H. (1976). *Mathematical Models in Plant Physiology*. Academic Press (Inc.)

London, Ltd.

United Nations Environment Programme (1992). World Atlas of Desertification.

      https://wedocs.unep.org/20.500.11822/42137.

Valentini, R., Arriga, N., Belelli, L., Dore, S., Manca, G., Mazzenga, F.,

      Pegoraro, E., Sabbatini, S., Stefani, P., Tirone, G., Vitale, D., Papale, D., Boschi, A., &

      Tomassucci, M. (2000-2008). FLUXNET2015 IT-Ro1 Roccarespampani 1

      [Dataset]. FLUXNET. https://doi.org/10.18140/FLX/1440174

Valentini, R., Dore, S., Mazzenga, F., Sabbatini, S., Stefani, P., Tirone, G., & Papale, D. (1997-

      2009). FLUXNET2015 IT-Cpz Castelporziano [Dataset]. FLUXNET.

      https://doi.org/10.18140/FLX/1440168

Varlagin, A., Kurbatova, J., & Vygodskaya, N. (1998-2014). FLUXNET2015 RU-

      Fyo Fyodorovskoye [Dataset]. FLUXNET. https://doi.org/10.18140/FLX/1440183

Wang, Y., Sperry, J. S., Anderegg, W. R. L., Venturas, M. D., & Trugman, A. T. (2020). A

      theoretical and empirical assessment of stomatal optimization modeling. *New*

      Phytologist, *227*(2), 311–325. https://doi.org/10.1111/nph.16572

Williams, M., Rastetter, E. B., Fernandes, D. N., Goulden, M. L., Wofsy, S. C., Shaver, G. R.,

      Melillo, J. M., Munger, J. W., Fan, S. M., & Nadelhoffer, K. J. (1996). Modelling the

      soil-plant-atmosphere continuum in a *Quercus-Acer* stand at Harvard Forest: The

      regulation of stomatal conductance by light, nitrogen and soil/plant hydraulic properties.

      Plant Cell, and Environment., *19*(8), 911–927. https://doi.org/10.1111/j.1365-

      3040.1996.tb00456.x

Wohlfahrt, G., Hammerle, A., & Hörtnagl, L. (2002-2012). FLUXNET2015 AT-Neu Neustift

      [Dataset]. FLUXNET. https://doi.org/10.18140/FLX/1440121

Wolf, A., Anderegg, W. R. L., & Pacala, S. W. (2016). Optimal stomatal behavior with

    competition for water and risk of hydraulic impairment. *Proceedings of the National*

    Academy of Sciences, *113*(46), E7222–E7230. https://doi.org/10.1073/pnas.1615144113

Woodgate, W., van Gorsel, E., Leuning, R., Kitchen, M., Hughes, D., & Zegelin, S. (2001-

    2014). FLUXNET2015 AU-Tum Tumbarumba [Dataset]. FLUXNET.

    https://doi.org/10.18140/FLX/1440126

Yamori, W., Hikosaka, K., & Way, D. A. (2014). Temperature response of photosynthesis in C_3,

    C_4, and CAM plants: Temperature acclimation and temperature adaptation.

    Photosynthesis Research, *119*(1), 101–117. https://doi.org/10.1007/s11120-013-9874-6

Yi, K., Maxwell, J. T., Wenzel, M. K., Roman, D. T., Sauer, P. E., Phillips, R. P., & Novick, K.

    A. (2019). Linking variation in intrinsic water-use efficiency to isohydricity: A

    comparison at multiple spatiotemporal scales. *New Phytologist*, *221*(1), 195–208.

    https://doi.org/10.1111/nph.15384

Yi, K., Smith, J. W., Jablonski, A. D., Tatham, E. A., Scanlon, T. M., Lerdau, M. T., Novick, K.

    A., & Yang, X. (2020). High heterogeneity in canopy temperature among co-occurring

    tree species in a temperate forest. *Journal of Geophysical Research: Biogeosciences,*

    125(12), e2020JG005892. https://doi.org/10.1029/2020JG005892

Zhang, Q., Ficklin, D. L., Manzoni, S., Wang, L., Way, D., Phillips, R. P., & Novick, K. A.

    (2019). Response of ecosystem intrinsic water use efficiency and gross primary

    productivity to rising vapor pressure deficit. *Environmental Research Letters, 14*(7),

    074023. https://doi.org/10.1088/1748-9326/ab2603

Zhou, S. X., Duursma, R. A., Medlyn, B. E., Kelly, J. W. G., & Prentice, I. C. (2013). How

    should we model plant responses to drought? An analysis of stomatal and non-stomatal

1294   responses to water stress. *Agricultural and Forest Meteorology*, *182–183*, 204–214.

1295   https://doi.org/10.1016/j.agrformet.2013.05.009

1296 Zhou, S. X., Medlyn, B., Sabate, S., Sperlich, D., & Prentice, I. C. (2014). Short-term water

1297   stress impacts on stomatal, mesophyll and biochemical limitations to photosynthesis

1298   differ consistently among tree species from contrasting climates. *Tree Physiology,*

1299   *34*(10), 1035–1046. https://doi.org/10.1093/treephys/tpu072